

## Original Article

# Apigenin ameliorates inflamed ulcerative colitis by regulating mast cell degranulation via the PAMP-MRGPRX2 feedback loop

Yihan Huang<sup>a,†</sup>, Na Wang<sup>b,†</sup>, Xiaolan Ji<sup>a</sup>, Shiqiong Luo<sup>a</sup>, Ling Gong<sup>a</sup>, Chenrui Zhao<sup>a</sup>, Guodong Zheng<sup>a</sup>, Rui Liu<sup>a,\*</sup>, Tao Zhang<sup>a,\*</sup>

<sup>a</sup> School of Pharmacy, Health Science Center, Xi'an Jiaotong University, Xi'an 710061, China

<sup>b</sup> Department of Otolaryngology, Affiliated Hospital of North China University of Science and Technology, Tangshan 063000, China



## ARTICLE INFO

## Keywords:

Ulcerative colitis  
Mast cells  
Carboxypeptidase A3  
apigenin  
MRGPRX2

## ABSTRACT

**Purpose:** The aim of this study was to investigate the therapeutic effect of API on UC via the regulation of PAMP-MRGPRX2-mediated mast cells (MCs) degranulation.

**Background:** The pro-inflammatory positive feedback loop mediated by Mas-related G-protein-coupled receptor X2 (MRGPRX2) and its endogenous ligand, PAMP-12, is associated with ulcerative colitis (UC) progression. However, the therapeutic strategies that target MRGPRX2 in the treatment of UC are less reported. Apigenin (API), a natural flavonoid, can relieve inflammation.

**Method:** A dextran sodium sulfate (DSS)-induced mouse UC model was used to elucidate the therapeutic effects of API. Animal behavior assessment, serological assays, and histological analysis were performed in wild-type (WT) and MC MrgprB2-conditional knockout (CKO) mouse model. mRNA sequencing analysis, PCR, ELISA, and western blotting were performed *in vitro* and *in vivo* to elucidate the mechanism underlying the effect of API by a PAMP-12 triggered MC degranulation model.

**Results:** MC degranulation via MrgprB2 was critical for the persistence of inflammation in colitis. API attenuated colonic tissue damage, splenomegaly, and myeloperoxidase (MPO) activity in the colonic tissues. It also ameliorated colonic crypt structure damage and inflammatory cell infiltration. Moreover, API suppressed MCs degranulation, and the level of carboxypeptidases A3 (CPA3), in DSS-induced colitis, thereby blocking the pro-inflammatory positive feedback loop induced by PAMP-MrgprB2. Lastly, API effectively inhibited PAMP-12-triggered mast cell degranulation by regulating Akt1/XBP-1S/CHOP/TXNIP and NF- $\kappa$ B/IL-1 $\beta$  signaling pathways.

**Conclusion:** API alleviates inflammatory symptoms in UC by suppressing PAMP-MRGPRX2/B2 mediated MC sustained degranulation feedback loop.

## Introduction

Ulcerative colitis (UC), a chronic inflammatory disease of the intestines, is a phenotype of inflammatory bowel disease (IBD) that begins in the rectum and successively spreads to the proximal part of the colon (de Lange and Barrett, 2015). Typical clinical manifestations include abdominal pain and discomfort, frequent defecation, bloody diarrhea

with mucus or pus, urinary urgency, weight loss, and urgency (Feuerstein and Cheifetz, 2014). The clinical treatment of UC aims to alleviate inflammatory symptoms (Turner et al., 2021). Pharmacological treatment is available for most patients with UC, with 5-Aminosalicylic acid (5-ASA), corticosteroids, immunomodulators, kinase inhibitors, and biologics being the primary therapeutic modalities (Mowat et al., 2011; Wehkamp et al., 2016). However, these treatments have

**Abbreviations:** 5-ASA, 5-aminosalicylic acids; ADM, adrenomedullin; Akt, protein kinase B; API, Apigenin; B2-CKO, MrgprB2-conditional knockout; CCK-8, Cell Counting-Kit-8; CHOP, C/EBP Homologous Protein; CPA3, carboxypeptidase A3; DAI, disease activity index; DAPI, 4',6-diamidino-2-phenylindole; DSS, Dextran Sulfate Sodium; ELISA, enzyme linked immol/Lunosorbent assay; FITC, Fluorescein isothiocyanate; GZMB, granzyme B; IBD, inflammatory bowel disease, IL-17RE, interleukin 17 receptor E; IL-8, interleukin-8; INF- $\gamma$ , interferon gamma; MC, Mast cells; MCP-1, monocyte chemoattractant protein-1; MPO, myeloperoxidase.

\* Corresponding authors.

E-mail addresses: [rliu2018@xjtu.edu.cn](mailto:rliu2018@xjtu.edu.cn) (R. Liu), [taozhang@xjtu.edu.cn](mailto:taozhang@xjtu.edu.cn) (T. Zhang).

† Yihan Huang and Na Wang contributed equally to this work.

<https://doi.org/10.1016/j.phymed.2025.156564>

Received 8 November 2024; Received in revised form 10 February 2025; Accepted 23 February 2025

Available online 1 March 2025

0944-7113/© 2025 Elsevier GmbH. All rights are reserved, including those for text and data mining, AI training, and similar technologies.

limitations such as a high incidence of adverse effects, high cost, and limited therapeutic ranges. For example, the 5-ASA analog sulfasalazine (Azulfidine) is the first-line treatment of UC that can be used to treat patients with extensive mild to moderately active UC, whereas 5-ASA analogs may be ineffective in patients with moderate to severe UC and are associated with various side effects, such as infertility, hemolytic anemia, photosensitivity, and agranulocytosis (Jeong et al., 2019). Therefore, identifying effective treatment options for UC remains essential.

Mast cells (MC) are important components of the intestinal barrier that respond to external and internal stimuli by expressing various receptors critical to intestinal homeostasis, such as those regulating mucosal integrity and epithelial barrier activity, as well as maintaining neuroimmune interactions that support the brain-gut axis (Albert-Bayo et al., 2019). Increased MC numbers, as well as degranulation, have been found at inflammatory sites in patients with UC. MC releases various active mediators, cytokines, and chemokines that can affect UC (Rijnijse et al., 2007). For example, its release of pro-inflammatory cytokines (interleukin-6 (IL-6) and interleukin-8 (IL-8)) and TNF- $\alpha$  plays a regulatory role in controlling the onset, progression, and resolution of intestinal inflammation (Boeckxstaens, 2015). Mas-related G-protein-coupled receptor X2 (MRGPRX2), a membrane receptor for MC, is activated by various ligands, including the endogenous neurotransmitter PAMP-12, prompting mast cells to release inflammatory mediators (Bawazir et al., 2022). MRGPRX2-mediated MC degranulation is associated with persistent inflammation in UC (Chen et al., 2021).

In the inflammatory region of UC, T cell-derived interferon  $\gamma$  (IFN- $\gamma$ ) induces MC degranulation to release carboxypeptidases A3 (CPA3), in turn, CPA3 hydrolyzes high levels of adrenal medullin (ADM) in UC to generate the neuropeptide, PAMP-12. The peptide then activates MC via MRGPRX2 to release CPA3, forming a pro-inflammatory positive feedback loop (Chen et al., 2021). This is an important factor that aggravates inflammatory symptoms and prolongs UC. However, blocking MRGPRX2-mediated MC degranulation for the treatment of UC has not been fully investigated. Further investigations are warranted to confirm the feasibility of this strategy prior to conducting subsequent drug development studies.

Apigenin (API) is a low-toxicity and beneficial bioactive flavonoid widely distributed in plants, fruits, and vegetables, with strong antioxidant, anti-inflammatory, anticancer, antiviral, antimicrobial, hepatoprotective, cardioprotective, and other pharmacological effects (Ginwala et al., 2019; Madunic et al., 2018; Salehi et al., 2019). The shallow binding pockets of MRGPRX2 contribute to the diversity of its ligands (Yang et al., 2021). Various flavonoids have been reported to inhibit MC degranulation via MRGPRX2 (Ding et al., 2019; Hao et al., 2022). Therefore, API may be a potential ligand for MRGPRX2 owing to its chemical and structural characteristics. Although API and its glycosides have been reported to alleviate UC (Li and Weigmann, 2023), the mechanism underlying UC alleviation by inhibiting MC activation remains unclear.

This project aimed to confirm the existence of a pro-inflammatory positive feedback loop involving PAMP-MRGPRX2 in UC and investigate the therapeutic effect and potential molecular mechanism of API in UC by suppressing PAMP-MRGPRX2 mediated MC degranulation. And it will provide novel insights into UC therapy by targeting mast cells and MRGPRX2.

## Materials and methods

### Reagents

DSS (60316ES60) was purchased from Yeasen Biotechnology Co., Ltd. (Shanghai, China); PAMP-12 and sulfasalazine (Azulfidine) were purchased from MedChemexpress Biotechnology Co., Ltd. (Shanghai, China); API was purchased from Baoji Chenguang Biotechnology Co., Ltd. (Baoji, China), with the purity  $\geq 98\%$ . p-Nitrophenyl N-acetyl- $\beta$ -D-

glucosamide and Triton X-100 were purchased from Sigma Aldrich Co., Ltd. (St. Louis, MO, USA). Pluronic F-127 and Fluo-3,AM were purchased from Biotium (California, USA). Saline was purchased from Shandong Qilu Pharmaceutical Co. Ltd. (Jinan, Shandong, China). Trizol lysate, RIPA lysate and chemiluminescent liquid (ECL) were purchased from Shanghai Epizyme Biomedical Technology Co., Ltd. (Shanghai, China). FITC-avidin (SF065) was purchased from Solarbio (Beijing, China); DAPI was purchased from BOSTER Biological Technology Co., Ltd. (Wuhan, China); anti-Akt1 (80,457-1-RR), anti-phosphorylated-Akt1 (Ser473, 80,462-1-RR) and anti- $\beta$ -actin (20,536-1-AP) were purchased from Proteintech (Wuhan, China); anti-NF- $\kappa$ B-P65 (#PTM-5591) was purchased from Jingjie Bioscience (Hangzhou, China); anti-phosphorylated-NF- $\kappa$ B-P65 (Ser536, #3033), anti-XBP-1S (#40,435), anti-PPAR- $\gamma$  (#2435) were purchased from Cell Signaling Technology (Danvers, MA); anti-IL-1 $\beta$  (A19635), anti-COX-2 (A3560) were purchased from ABclonal (Wuhan, China); anti-CHOP (CY6694), anti-TXNIP (CY7216) were purchased from Shanghai Ebiwei Biotechnology Co., Ltd (Shanghai, China). Mk-459 Millipore Milli-Q Plus ultrapure water system was used to obtain ultrapure water for use in all aqueous solutions. StemPro-34 medium were purchased from Invitrogen (California, USA); StemPro Nutritional Supplement were purchased from Invitrogen (California, USA); human stem cell factor and mice stem cell factor were purchased from Novoprotein Scientific Inc (Suzhou, China); L-glutamine were purchased from Sino Biological Co., Ltd (Beijing, China); penicillin-streptomycin were purchased from MedChemexpress Biotechnology Co., Ltd. (Shanghai, China); DMEM medium were purchased from Invitrogen (California, USA); fetal bovine serum (FBS) were purchased from Gibco (California, USA).

### Animals

Mouse MrgprB2 and human MRGPRX2 are homologous genes (McNeil et al., 2015). MRGPRX2 and MrgprB2 are expressed not only in mast cells, but also in dorsal root ganglion (Wu et al., 2015). C57BL/6-Tg (Cpa3-cre)4Glli/J mice were reported to be severely deficient in mast cells and basophils, while the number of other hematopoietic cell populations was virtually unchanged (Lilla et al., 2011). We constructed C57BL/6-MrgprB2(flox/flox) mice and bred them with C57BL/6-Tg (Cpa3-cre) Glli/J mice to obtain mast cells and basophils MrgprB2-conditional knockout (CKO) mice.

The C57BL/6-Tg(Cpa3-cre)4Glli/J mice (Strain<sup>#</sup>:026,828) were purchased from The Jacksons Laboratory from the official website (<https://www.jax.org/strain/026828#>). The C57BL/6-MrgprB2(flox/flox) mice were constructed by GemPharmatech Co., Ltd. (Item number: GFW0109121346-01). C57BL/6 mice were purchased from Xi'an Jiaotong University (Xi'an, China), and MC deficient Kit<sup>W-sh/W-sh</sup> mice were purchased from Nanjing University (Nanjing, Jiangsu Province, China).

All the mice were housed in a specific pathogen-free (SPF) grade laboratory animal center of Xi'an Jiaotong University. The phenotypes of the mice were identified by PCR and agarose gel technique, and the identification results were shown in Supplementary Figure 1 and Supplementary Figure 2.

Kit<sup>W-sh/W-sh</sup> mice PCR identification primer sequence are:

F: 5'-AGGCTTGAGCGCATTAT-3';

R: 5'-GAGGATTCATAGTTGTTCAATGTC-3'.

MrgprB2-CKO mice PCR identification primer sequence are:

F: 5'-ACTGTTCCATCCCCAGGAACC-3';

R: 5'-CCAGTTCTGCGAACCTCAT-3'.

6–8 weeks-old mice were used for the experiments, and all animal experiments were approved by the Ethics Committee of Xi'an Jiaotong University (Animal Experimentation Ethics No XJTUAE2023-1624), and the experiments were conducted in accordance with the Guide for the Care and Use of Laboratory Animals.

### Mouse UC model establishment

The mouse UC models were established by allowing them to freely consume a 5 % (w/v) DSS aqueous solution for 5 consecutive days, following the protocols outlined in previous studies (Wirtz et al., 2007, 2017). For demonstrating the role of mast cell and MrgprB2 in UC, the WT mice, Kit<sup>W-sh/W-sh</sup> mice, and MC MrgprB2 conditioned knockout (B2-CKO) mice, were randomly divided into two groups ( $n = 6$ ). The NOR groups were negative control group, and these mice drank normal water. While the UC groups were the model groups, and those mice drank water containing DSS. The weight of mice in each group was recorded before establishing the model.

For investigating the therapeutic effects of API, the C57BL/6 mice were randomly divided into six groups ( $n = 6$ ), which included normal group (NOR), model group (UC), sulfasalazine (Azulfidine) group (100 mg/kg SASP) group, 10 mg/kg API group (API 10), 20 mg/kg API group (API 20), and 40 mg/kg API group (API 40). The mice in UC group, SASP group, and API group, freely drank 5 % (W/V) DSS aqueous solution. The mice in the NOR groups freely drank normal water. Saline (0.2 ml/day) was applied to each mouse by gavage administration in NOR and UC groups. SASP, or API, was applied to the mice in NOR and UC groups (0.2 ml/day), respectively. All the mice were euthanized on the sixth day of modeling.

### Disease activity index assessment

During the modeling period, mice were weighed and recorded at the same time every day, and fecal samples were collected to assess stool consistency and the presence of blood. Scoring was conducted by experimenters blinded to the group allocation to evaluate the Disease Activity Index (DAI) daily (Yan et al., 2018), following the criteria outlined in Table 1.

### Macroscopic damage score

After euthanizing, any signs of rectal bleeding (blood at the anal opening) or rectal prolapse were meticulously recorded for each mouse. Following the removal of colonic tissues, observations were made regarding fecal consistency and bleeding within the colorectum (Yan et al., 2018). The scoring criteria are presented in Table 2.

### Myeloperoxidase (MPO) activity assay

In accordance with the existing assay method, the tissue homogenate was prepared by adding the appropriate amount of HTAB buffer according to the wet weight of the colon tissue (for tissue weight <25.00 mg, add buffer at 12.50 mg/ml; for 25.00 mg < tissue weight ≤ 50.00 mg, add buffer at 25.00 mg/ml; and so on) (Kim et al., 2012). A volume of 7 μl of the tissue homogenate supernatant was added in triplicate to a 96-well plate, and then add 50 μl of diluted H<sub>2</sub>O<sub>2</sub> (4 μl of 30 % H<sub>2</sub>O<sub>2</sub> diluted in 96 μl of ddH<sub>2</sub>O) to 100 ml of the freshly prepared o-dianisidine dihydrochloride solution. The o-dianisidine dihydrochloride solution containing H<sub>2</sub>O<sub>2</sub> was obtained. Using a multichannel pipette, 200 μl of the H<sub>2</sub>O<sub>2</sub>-containing o-dianisidine dihydrochloride solution was added to each well with tissue homogenate supernatant, and the

**Table 1**  
Disease activity index rating scale.

score	weight loss	faecal consistency	hemorrhage
0	no reduction	normal	normal
1	1–5 %		
2	5–10 %	meager stool	Occult bleeding (blood in the faeces)
3	10–20 %		
4	>20 %	constipation	Haemorrhage (blood around the anus)

**Table 2**  
Macro impairment scoring scale.

score	rectum bleeding	rectal prolapse	stool consistency	colon bleeding
0	no bleeding	no prolapse	normal	normal
1	rectum red	minor prolapse	soft	red colon
2	rectum Crimson	obvious prolapse	Very soft	Crimson colon
3	rectum hemorrhage	wide prolapse	have the runs	black colon

absorbance at 450 nm was measured immediately by a FlexStation@3 enzyme marker. The initial absorbance was detected and readings were taken at 30-second intervals over a one-minute period, and the absorbance was recorded at three-time points,  $t_{0s}$ ,  $t_{30s}$ , and  $t_{60s}$ , and the MPO activity was quantified as units (U) of MPO/mg of tissue.

### Measurement of CPA3 and ADM in colon tissue

Based on the wet weight of the tissue, lysis buffer was added to each colon tissue sample at a weight-to-volume ratio of 1:9 (1 g of tissue to 9 ml of solution). Homogenization beads were then added to each sample tube, and tissues were homogenized using a high-throughput tissue homogenizer for approximately 10 min at 70 Hz to ensure complete tissue disruption and obtain the tissue homogenate. The samples were subsequently centrifuged at  $3300 \times g$  for 5 min at 4 °C, aspirate the supernatant, remove the homogenizing beads and discard the precipitate. The supernatant was carefully aspirated, the homogenizing beads were removed, and the precipitate was discarded. The collected supernatant can be stored at –80 °C until further analysis. ELISA kits were used to measure the levels of CPA3 and ADM in the colon tissue lysates from each group of mice, following the manufacturer's instructions strictly.

### Histamine determination

Tissue homogenate supernatant or cell supernatant with a volume of 50 μl was evenly mixed with histamine internal standard with a volume of 100 μl, centrifuged at 4 °C at 12,000 rpm for 20 min, and the supernatant was carefully collected. The resulting supernatant was filtered through a 0.22 μm organic filter membrane for histamine content analysis by mass spectrometry (Han et al., 2017).

### Hematoxylin & Eosin (H&E) staining

The freshly excised colon tissues were immediately fixed with 4 % paraformaldehyde for 24 h. At the end of fixation, the tissues were sequentially immersed in graded ethanol series for dehydration, permeabilized by xylene, and then embedded in paraffin wax, and the paraffin sections with a thickness of 5 μm were cut. Then the sections were sequentially immersed in xylene solution twice for 8 min/times, and in anhydrous ethanol twice for 6 min/times, and then in 95 %, 85 %, and 75 % alcohol solution for 5 min, and rinsed with tap water. Hematoxylin staining was performed for 5 min. Next, the sections were stained for 5 min with 1 % hydrochloric acid in alcohol, followed by immersion in 75 % alcohol solution for 5 min, and rinsed with tap water. After staining with hematoxylin alkaline dye for 5 min, the previous rinsing step was repeated. The sections were then differentiated briefly with 1 % hydrochloric acid in alcohol, rinsed with tap water, and restored to blue using running water. Following eosin staining for 2 min, excess dye was rinsed away with tap water. The sections were then sequentially immersed in 75 % and 85 % alcohol solutions for 30 s each, followed by two immersions in 95 % alcohol and two immersions in anhydrous ethanol, each lasting 5 min. The sections were then immersed in xylene solution twice and dehydrated until the tissue became completely transparent. After removal and drying, the sections were

sealed with neutral resin and observed under a microscope. Photographs were taken for documentation.

#### Immunofluorescence staining

Immunofluorescence staining was employed to detect mast cell infiltration in the colon tissues of mice. Paraffin sections, 5  $\mu\text{m}$  thick, were prepared and dewaxed to water following the protocol outlined above. The sections were incubated in citrate buffer (pH 6.0) for 2 min to perform antigen retrieval. The sections were washed with PBS and subsequently blocked with 1 % BSA for 30 min at room temperature. The primary antibody, Avidin (Solarbio, SF065), was diluted at a 1:200 ratio and applied dropwise to the sections in a humidity chamber at 4  $^{\circ}\text{C}$ , protected from light. After washing with PBS, the sections were stained with DAPI, incubated at room temperature for 10 min, and excess stain was removed by rinsing with PBS. The sections were then mounted with glycerol and observed under a confocal microscope for imaging.

#### Cell culture

LAD2 cells employed in this study were graciously supplied by researchers A. Kirshenbaum and D. Metcalfe from the National Institutes of Health (NIH) in the USA. These cells were maintained in StemPro-34 medium, which includes StemPro Nutritional Supplement, 100 ng/ml of human stem cell factor, 2 mmol/l of l-glutamine, and 100 U of penicillin-streptomycin.

HEK293-MRGPRX2 cells, which were initially constructed in our laboratory, were grown in Dulbecco's Modified Eagle Medium (DMEM) supplemented with 10 % Fetal Bovine Serum (FBS) and 100 U of penicillin-streptomycin. Additionally, HEK293 cells were cultured in DMEM with 10 % FBS and 100 U of penicillin-streptomycin.

Mouse peritoneal mast cells (MPMC) were purified by isotonic 70 % Percoll suspension after ice-cold mast cell dissociation media lavages in the peritoneum (Liu et al., 2017), and nurtured in DMEM containing 100 U of penicillin-streptomycin, 10 % FBS, and 25 ng/ml recombinant mouse stem cell factor.

#### Molecular docking

The Surflex-Dock module within the SYBYL-X 2.0 software suite (Tripos, St. Louis, MO, USA) was employed to investigate the interactions between receptors and ligands. For this purpose, molecular docking studies were conducted to explore the binding affinity between MRGPRX2 and API. The MRGPRX2 protein structure, retrieved from the Protein Data Bank (PDB) with the accession code 7S8 N (<https://www.rcsb.org/>).

#### Surface plasmon resonance assay

MRGPRX2 (Sino Biological, Inc.) proteins were prepared at a concentration of 25  $\mu\text{g}/\text{ml}$  according to the standard operating instructions of the Open SPRTM instrument. The proteins were then coupled and immobilized on a CM5 sensor chip (Cytiva Sweden AB, Uppsala, Sweden) as per the manufacturer's instructions to create an MRGPRX2 chip. The binding affinity between the ligand and receptor was assessed using the Biacore T200 Molecular Interaction Analysis System, adhering to the standard operating instructions for the Open SPR™ instrument. A series of API concentrations, ranging from high to low (100  $\mu\text{mol}/\text{l}$ , 50  $\mu\text{mol}/\text{l}$ , 25  $\mu\text{mol}/\text{l}$ , 12.5  $\mu\text{mol}/\text{l}$ , 6.25  $\mu\text{mol}/\text{l}$ , and 3.125  $\mu\text{mol}/\text{l}$ ), were injected into the system to measure the interaction with MRGPRX2. The binding phase was set for 180 s, while the dissociation phase was set for 600 s, in accordance with the operational manual. The flow rate was maintained at 20  $\mu\text{l}/\text{s}$  throughout the analysis. Finally, the data were processed by TraceDrawer™ software and  $K_D$  values were calculated.

#### Calcium imaging assay

Four kinds of cell lines were employed to assess the inhibition effect of API on MRGPRX2 by calcium imaging assay. HEK293 cells were applied as a blank control group. HEK293 cells were seeded into a 96-well plate at a density of 4000 cells per well, and these cells were cultured in the incubator overnight to allow the cells to adhere to the plate. Then the culture medium was removed, and the cells were washed twice with CIB, and then CIB was discarded. The cells were incubated with calcium fluorescence incubation solution for 30 min in the incubator at 37  $^{\circ}\text{C}$  and saturation humidity. The calcium fluorescence incubation solution was prepared freshly by diluting Fluo,3-AM and F-127 with CIB at the ratio of 1:2000 and 1:4000, respectively. After the 30 min incubation, the solution was removed and the cells were washed twice with CIB. Cells in the plate were put under the view of a fluorescence microscope (Nikon ECLIPSE Ti-S). In the same field of view, the FITC (green) fluorescence signal intensity changes of the observed cells were recorded within 120 s. Set the fluorescence microscope to take a photo every 1 s. Add the agonist at the 5-second mark when the photo-taking begins. After the experiment, the data was analyzed by the NIS-Elements AR Analysis software (4.50.00), the target cells were selected, and the fluorescence intensity of the specific cells was calculated in 120 s. After the background fluorescence value was removed, statistical analysis was performed. The curve of fluorescence intensity of cells over time and the bar graph of the difference between maximum and minimum fluorescence intensity of cells within 120 s were drawn. CIB alone, 20  $\mu\text{mol}/\text{l}$  API, and 4  $\mu\text{mol}/\text{l}$  PAMP-12 were applied as agonists in HEK293T cells to confirm that they don't activate the cells. The activation effect of CIB alone and 20  $\mu\text{mol}/\text{l}$  API on HEK293-MRGPRX2 cells were also applied as another control groups, and the densities of HEK293-MRGPRX2 cells were same to HEK293T cells. In order to explore the antagonistic effect of API on MRGPRX2, 5  $\mu\text{mol}/\text{l}$ , 10  $\mu\text{mol}/\text{l}$ , or 20  $\mu\text{mol}/\text{l}$  API was added to the calcium fluorescence incubation solution and pre-treated for 30 min. Then 4  $\mu\text{mol}/\text{l}$  PAMP-12 was used as an agonist to trigger the influx of extracellular calcium ions. MPMC and LAD2 cells are suspension cells, these cells were seeded into the 96-well plate at a density of 5000 cells per well, and they were washed with CIB by centrifugation. The cells were incubated immediately with 5  $\mu\text{mol}/\text{l}$ , 10  $\mu\text{mol}/\text{l}$ , or 20  $\mu\text{mol}/\text{l}$  API mixed in the calcium fluorescence incubation solution for 30 min. After washing with CIB, the cells were triggered by 4  $\mu\text{mol}/\text{l}$  PAMP-12, and recorded the fluorescence signal intensity changes of the cells. The data analysis was same to adherent cells. The activation effect of CIB alone on MPMC and LAD2 cells were also applied as blank control groups.

#### $\beta$ -hexosaminidase release rate determination assay

LAD2 cells were inoculated into 96-well plates at a rate of 5000 cells per well, centrifuged to discard the medium, 50  $\mu\text{l}$  of TM buffer with varying concentrations of API was added to the wells designated for the API group. The PAMP-12 group and the blank control group received 50  $\mu\text{l}$  of TM buffer without API. The plates were then incubated in a cell culture incubator for 30 min. Following the initial incubation, 50  $\mu\text{l}$  of TM buffer containing 4  $\mu\text{mol}/\text{l}$  PAMP-12 was added to both the API and PAMP-12 groups, while an equal volume of TM buffer was added to the blank control group. The plates were incubated for an additional 30 min. After incubating, 50  $\mu\text{l}$  of TM buffer containing 4  $\mu\text{mol}/\text{l}$  PAMP-12 was added to the API group and the PAMP-12 group, and an equal volume of TM buffer was added to the blank control group, and the plates were further incubated for 30 min. At the end of the incubation, the 96-well plate was removed, and 50  $\mu\text{l}$  of the cell supernatant was aspirated into a new 96-well plate after centrifugation. The remaining supernatant was discarded, and 100  $\mu\text{l}$  of 0.1 % Triton X-100 lysis solution was added to the blank control group to lyse the cells. After centrifugation, 50  $\mu\text{l}$  of the lysate supernatant was collected from the blank control wells. Sequentially add 50  $\mu\text{l}$  of  $\beta$ -aminohexose solution to all the supernatants

and incubate for 90 min at 37 °C. Wait for the incubation to complete, add 150 µl of termination solution to terminate the reaction, and then immediately use an enzyme marker to detect the OD value at 405 nm.

#### Enzyme-linked immunosorbent assay (ELISA)

LAD2 cells were inoculated into 96-well plates according to 5000 cells per well, centrifuged to discard the medium, 80 µl of TM buffer containing different concentrations of API was added to the API group, and 80 µl of TM buffer was added to the wells of the PAMP-12 group and the blank control group, and the plates were incubated in an incubator for 30 min; the 96-well plates were taken out at the end of the incubation, and 80 µl of TM buffer containing 4 µmol/l PAMP-12 was added to the API group and PAMP-12 group, and an equal volume of TM buffer was added to the blank control group. After incubation, remove the 96-well plate, add 80 µl of TM buffer containing 4 µmol/l PAMP-12 to the API group and the PAMP-12 group, add an equal volume of TM buffer to the blank control group, and continue to incubate for 6 h. After incubation, remove the 96-well plate, and centrifuge to collect 120 µl of cellular supernatant into the corresponding EP tubes. The levels of degranulating substance CPA3 and released TNF-α, IL-8, and MCP-1 from LAD2 cells were detected in strict accordance with the instructions provided by the reagent manufacturer.

#### Real time PCR assay

LAD2 cells at a density of  $5 \times 10^6$  cells/ml were inoculated into 6-well plates, and API was added to make the final concentrations of API in the cell suspension 5 µmol/l, 10 µmol/l, and 20 µmol/l. The cells were incubated in an incubator for 30 min, and then PAMP-12 was added to the PAMP-12 group and the API group to make the final concentration in the cell suspension 2 µmol/l. The incubation was extended for an additional 30 min. Subsequently the cells were centrifuged in 1.5 ml EP tubes to remove the medium washed twice with RNase-Free PBS, and centrifuged again to collect the cell pellet. 1 ml of Trizol solution was added to the cell precipitate to lyse the cells, and the cells were left at room temperature for 5–10 min to be completely lysed. Total RNA was extracted using the Trizol method, and RNA extraction was continued following the manufacturer's instructions. Once the mRNA concentration was determined, the expression of cytokines was assessed using an RT-PCR kit. Primers, synthesized by AUKO Biologicals, were utilized for this purpose, with the specific primer sequences detailed in Table 3.

#### mRNA sequencing analysis

LAD2 cells with a density of  $5 \times 10^6$  cells/ml were inoculated into 6-well plates, and API was added to make the final concentrations of API in the cell suspension 5 µmol/l, 10 µmol/l and 20 µmol/l. The cells were incubated in an incubator for 30 min, and then PAMP-12 was added to the PAMP-12 and API groups to make the final concentration of 2 µmol/l. The incubation was continued for 3 h. After incubation, the 6-well plates were removed, and the cell suspension was aspirated into the corresponding 1.5 ml EP tubes. After incubation for 3 h, remove the 6-well plate, aspirate the cell suspension into the corresponding 1.5 ml EP tubes, centrifuge to discard the medium, wash twice with RNase-Free PBS, and centrifuge to obtain the cell precipitate; lysed the cells by adding Trizol solution, and then placed at room temperature for 5–10 min to be used until the cells were completely lysed, and then transferred to a freezing tube to be preserved at –80 °C.

The experiment was entrusted to Lianchuan Biotechnology Co., Ltd. for subsequent on-line and basic data analysis. The samples were tested and analyzed for correlation, differentially expressed genes, differentially expressed gene function and pathway annotation and KEGG enrichment analysis. After obtaining the data, the data were mined and analyzed according to the demand.

**Table 3**

Sequence of primers for genes to be tested.

Gene name	primer sequence
CPA3 Forward	CATCACCTTCCATTCTACTCC
CPA3 Reverse	gTTgATAgAACATCAgTgCCAATC
MCP-1 Forward	gTCCCAAAGAAgCTgTgATCT
MCP-1 Reverse	AgTCTTCggAgTTTgggTTTg
TNF-α Forward	CCTggTATgAgCCCATCTATCT
TNF-α Reverse	CAGggCAATgATCCCAAAGT
IL-8 Forward	CTgCgCCAACACAgAAATTAT
IL-8 Reverse	AAACTTCTCCACAACCCTCTg
GAPDH Forward	CTCCTCCACCTTTgACgCTg
GAPDH Reverse	TCCTCTTgTgCTCTTgCTg
CHOP Forward	AgCgCATgAAgAgAAAgAA
CHOP Reverse	TCACCATTTCgTCAATCAgAg
XBPI Forward	CAGTgAAgAgAACTgTgTAAg
XBPI Reverse	CATCCAgTAggCAGgAAgATg
TXNIP Forward	CCTTCgggTTCAGAAgATCAg
TXNIP Reverse	ggATCCAggAACgCTAAACATAg
NF-κB Forward	gAgACATCCTTCCgCAAACT
NF-κB Reverse	ggTCCTTCTgCCCATAATC
IL-1β Forward	ggTgTTCTCCATgTCTCTTgTA
IL-1β Reverse	CTgTAgAgTgggCTTATCATC
GZMB Forward	ACACTCACACACTACAAGAg
GZMB Reverse	ACgCACAACTCAATggTACT
IL-17RE Forward	CACACTgTAgAgCTgCCTTATg
IL-17RE Reverse	CAGCTCTgAAgggACATTT
GAPDH Forward	CTCCTCCACCTTTgACgCTg
GAPDH Reverse	TCCTCTTgTgCTCTTgCTg

#### Western blotting assay

LAD2 cells at a density of  $5 \times 10^6$  cells/ml were inoculated into 6-well plates, and API was added to the cell suspension to achieve final concentrations of 5 µmol/l, 10 µmol/l and 20 µmol/l. The cells were incubated in a 37 °C incubator for 30 min, and then PAMP-12 and API groups were added to achieve final concentrations of 2 µmol/l PAMP-12, and the cells were continued to be incubated for 6 h. After the incubation, the total cell protein was obtained after a series of steps according to the instructions, and the protein concentration was tested by a BCA kit. Then boiling the proteins at 100 °C for 5 min after mixing with loading buffer. After electrophoresis and membrane transfer, the proteins were attached to the cellulose acetate membrane. The membrane was incubated with 5 % skim milk powder buffer, and then incubated with different primary antibodies overnight at 4 °C. The primary antibodies included anti-Akt1 (1:1000), anti-phosphorylated-Akt1 (1:1000), anti-XBP-1S (1:1000), anti-CHOP (1:1000), anti-TXNIP (1:1000), anti-NFκB-P65 (1:1000), anti-phosphorylated-NFκB-P65 (1:1000), anti-IL-1β (1:1000) and anti-β-actin (1:1000). After cleaning, the membranes were incubated with the secondary antibody at room temperature for 2 h. The target proteins were then colored by ECL luminescent solution and were photographed using a chemiluminescence instrument. The grayscale of each target protein was analyzed using Image J software after photographing.

#### Statistical analysis

The preliminary processing of the data was carried out using Excel, and the processed experimental data were analyzed using GraphPad Prism 8.3.4 software (GraphPad Software Inc., San Diego, CA). The normality of the data was assessed using the Shapiro-Wilk test. Statistical comparisons were conducted via one-way ANOVA, followed by *post hoc* analyses: the least significant difference (LSD) test or the Tamhane's t-test were employed in appropriate circumstances. Data were expressed as mean ± standard error of the mean (SEM), and statistically significant were considered as  $p < 0.05$ .

**Results**

*MC and MrgprB2 exacerbate inflammatory symptoms in mice with acute UC*

The DSS-induced mouse UC model was built from day 1 to day 5. On day 6, the mice were euthanized after behavioral observation, and serum and colon tissues were collected for serological and histopathological analysis (Fig. 1A). During the modeling process, the DAI scores of body weight, fecal consistency and fecal blood in each group were recorded (Fig. 1B), and the higher scores indicated more severe disease symptoms. Compared to WT mice, the DAI score increase trend were flatter in Kit<sup>W-sh/W-sh</sup> mice and B2-CKO mice, indicating slower disease progression (Fig. 1C). Furthermore, diarrhea and colonic bleeding symptoms in Kit<sup>W-sh/W-sh</sup> and B2-CKO mice were alleviated to varying degrees (Fig. 1D, E). The macroscopic damage scores of the colonic tissues further demonstrated that the colonic damage was less severe in Kit<sup>W-sh/W-sh</sup> mice and B2-CKO mice compared to that in WT mice (Fig. 1F). We compared the colon lengths across the different mouse groups and discovered that, within the UC model, WT mice, Kit<sup>W-sh/W-sh</sup> mice, and B2-CKO mice exhibited varying degrees of colon shortening subsequent to consuming water containing DSS (Fig. 1G). In addition, through the detection of MPO activity, it was found that the MPO levels were elevated in the colonic tissues of mice in the UC model groups

(Fig. 1H).

We calculated the increased multiples of MPO activity in UC mice and compared them with those in NOR mice for each genotype, and the increase of MPO activity was calculated by equation 1 ( $M = (S_{UC} - S_{NOR}) / S_{NOR}$ ). In formula 1, M represented the MPO activity increase ratio, S<sub>UC</sub> represented the MPO detection value in UC groups, and S<sub>NOR</sub> represented the MPO detection value in MOR groups. The results showed that the increase in MPO activity was greater in WT mice compared to Kit<sup>W-sh/W-sh</sup> and B2-CKO mice (Fig. 1I). Therefore, in the established UC models, the symptoms of Kit<sup>W-sh/W-sh</sup> and B2-CKO mice were relatively milder compared to those of WT mice, and MC and MrgprB2 play a role in promoting inflammatory responses in the acute mouse model of UC.

*PAMP-MrgprB2-MC positive feedback loop exacerbates the inflammatory symptoms in acute UC*

The H&E staining results of the colon tissue of mice showed that the colon structure of the NOR group mice was intact and there were no inflammatory pathological changes. In UC model mice, the colon structure of WT mice was severely damaged, with the disappearance of crypt structures and infiltration of inflammatory cells. However, the colonic structure of the UC group in Kit<sup>W-sh/W-sh</sup> mice and B2-CKO mice was relatively intact, with less infiltration of inflammatory cells (Fig. 2A). In addition, avidin immunofluorescence staining showed

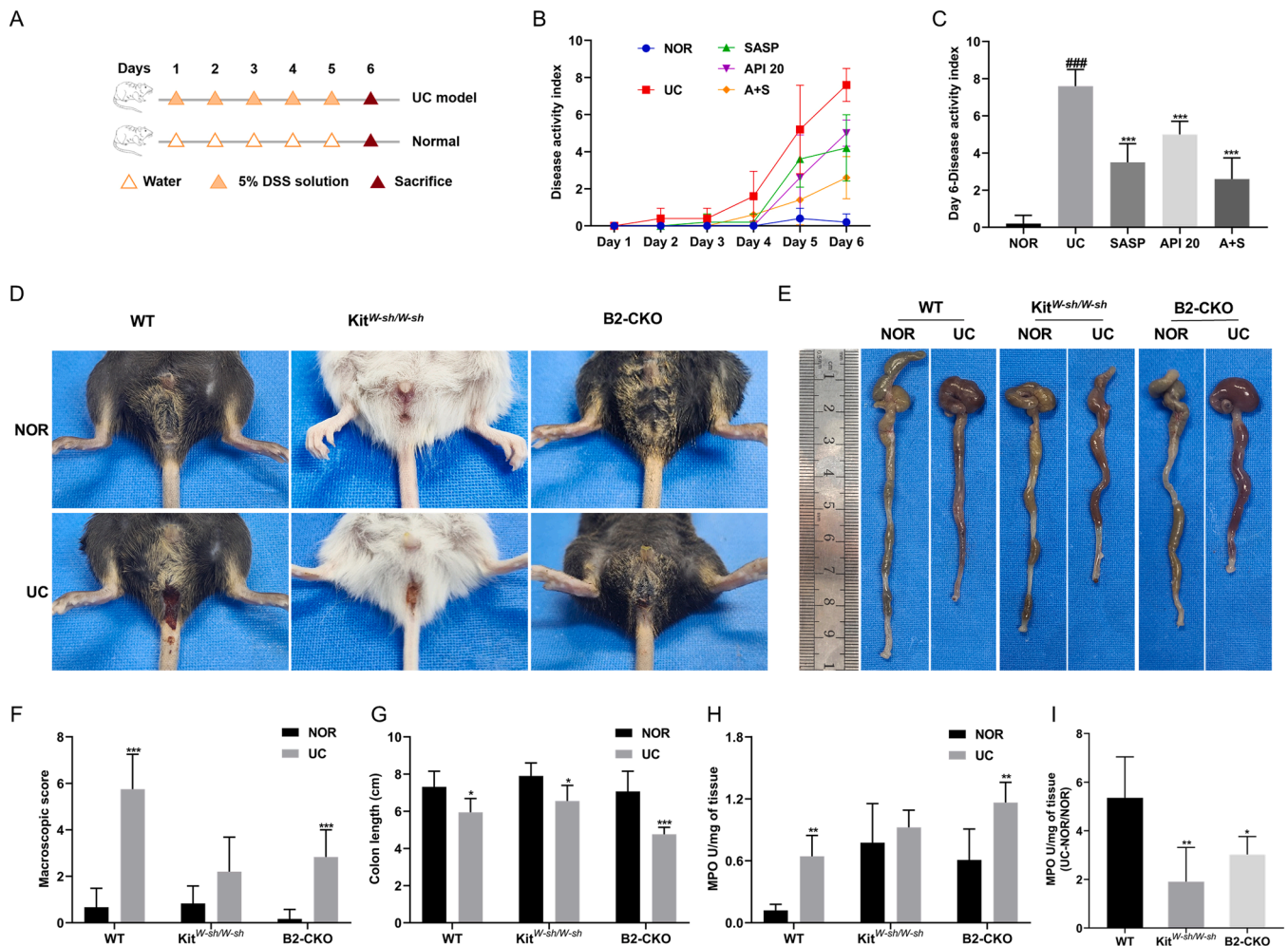


**Fig. 1.** Study of inflammatory symptoms in different genotypes of mice (A) Methods of establishing the mouse model of colitis. (B) Mouse disease activity index. (C) Statistical analysis of the disease activity index in mice on day 6. (D) Representative diagrams of diarrhea in each group of mice. (E) Representative diagrams of colon in each group of mice. (F) Macroinjury scores. (G) Length of mouse colon. (H) Measurement of peroxidase (MPO) activity. (I) Multiplicity of increase in MPO activity (vs. NOR group, \**p* < 0.05, \*\**p* < 0.01, \*\*\**p* < 0.001, *n* = 6).

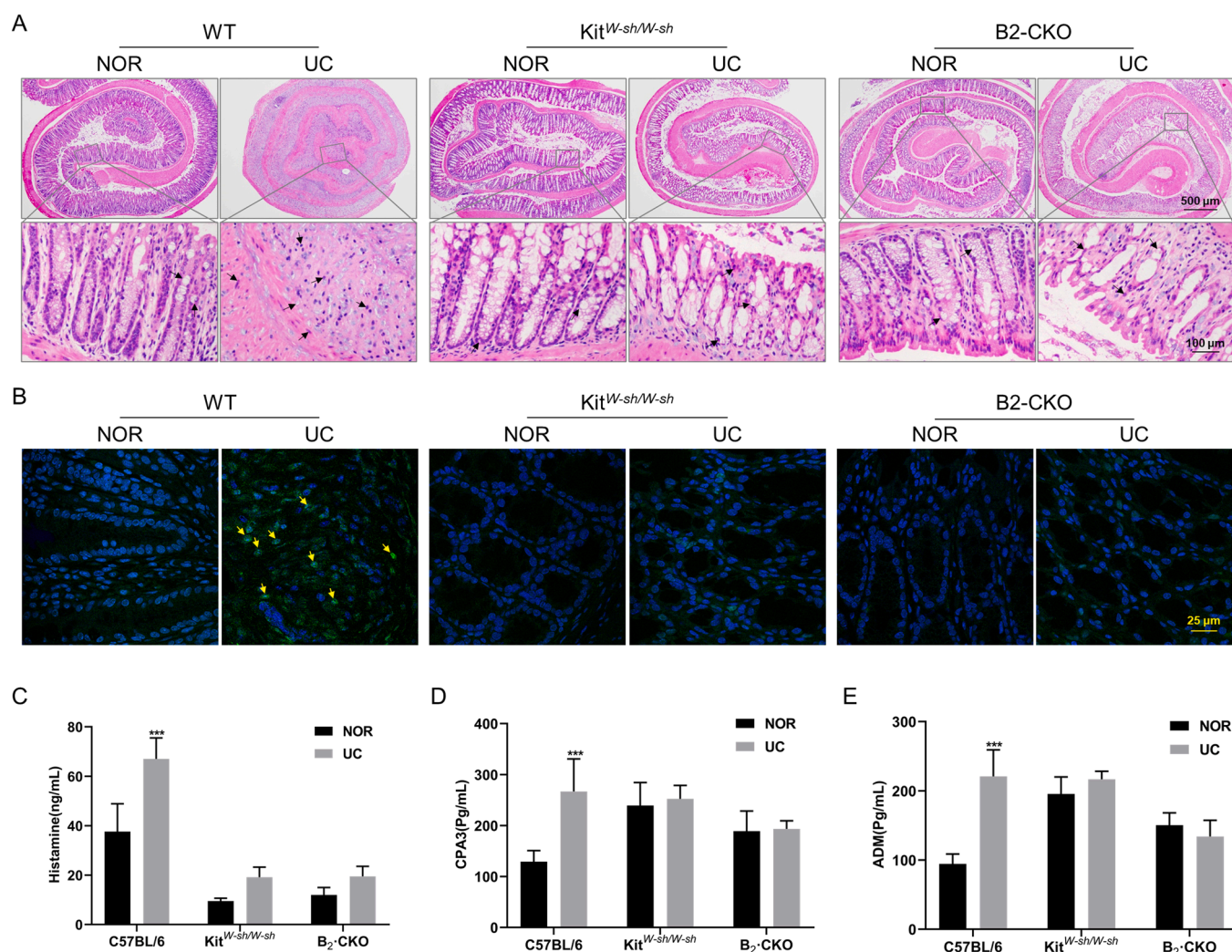


**Fig. 2.** Tissue damage in the colon of mice of different genotypes

(A) Structural and morphological diagram of mouse colon tissues under microscope, and the lower pictures were the magnified pictures in the grey boxes of the upper pictures. The black arrows in the figures indicate the representative crypt structure and inflammatory cell infiltration in the colonic tissue. (B) Results of Avidin (green) and DAPI (blue) staining of mouse colon tissues. The yellow arrows marked representative avidin-stained MCs. (C) Detection results of histamine in mouse colon tissues. (D) Detection results of CPA3 in mouse colon tissues. (E) Detection results of ADM in mouse colon tissues (vs. NOR group, \*\*\* $p < 0.001$ ,  $n = 6$ ).

strong green fluorescence in the colon tissues of WT mice in the UC model, while Kit<sup>W-sh/W-sh</sup> mice and B2-CKO mice did not. This suggests that MCs have increased infiltration into the colon tissue of UC mice and are involved in regulating the inflammatory response of the colon (Fig. 2B). By detecting the contents of histamine, CPA3, and ADM in the lysates of colon tissues from each group, it was found that the concentrations of these mediators in the colon tissues of WT mice in UC model significantly increased, while there was no significant increase in Kit<sup>W-sh/W-sh</sup> mice and B2-CKO mice (Fig. 2C–E). In the UC model, the level of ADM increased in colon tissue, and CPA3 released upon mast cell (MC) activation could be hydrolyzed by ADM to generate PAMP-12, which was an endogenous ligand for MrgprB2/X2. Consequently, PAMP-12 can activate MCs via MrgprB2/X2, leading to the release of CPA3 once again. This established a positive feedback loop of PAMP-MrgprB2-MC in colon tissue that continuously activated MCs, thereby promoting inflammatory responses in UC. However, in mice with MC dysfunction or MrgprB2 knockout, this positive feedback loop was disrupted, resulting in milder inflammatory symptoms of UC in these mice. These findings suggested that targeting MCs and MrgprB2/X2 might be a new potential therapeutic strategy for UC.

*API is a natural active ingredient that can alleviate the inflammatory symptoms of UC in mice*

Considering the structure of API (Fig. 3A) and its significant potential in the treatment of UC, we constructed an acute DSS-induced UC mouse model to investigate its therapeutic effects (Fig. 3B). The DAI scoring results revealed that the score values of mice in UC group were significantly elevated, while the score values of mice in NOR group remained at 0. In contrast, the score values of mice in the API and SASP groups increased slowly, indicating slower progression of UC in the treatment groups (Fig. 3C). On the sixth day, after euthanizing the mice, DAI scores were assessed for each group. The results demonstrated that both 40 mg/kg of API and 100 mg/kg of SASP exhibited significant antagonistic effects against UC (Fig. 3D). Additionally, by observing the anus of the mice, it was found that there was a reduction in diarrhea and colonic bleeding in these two groups (Fig. 3E, F). The macroscopic scoring results for colonic tissue inflammation symptoms showed that, compared with the UC group, colonic damage was significantly reduced under treatment of API and SASP. Specifically, the effects of 40 mg/kg API in alleviating UC symptoms were comparable to those of 100 mg/kg SASP (Fig. 3G). Meanwhile, statistical analysis of the colonic lengths of mice in each group revealed that the colonic length of mice in UC group

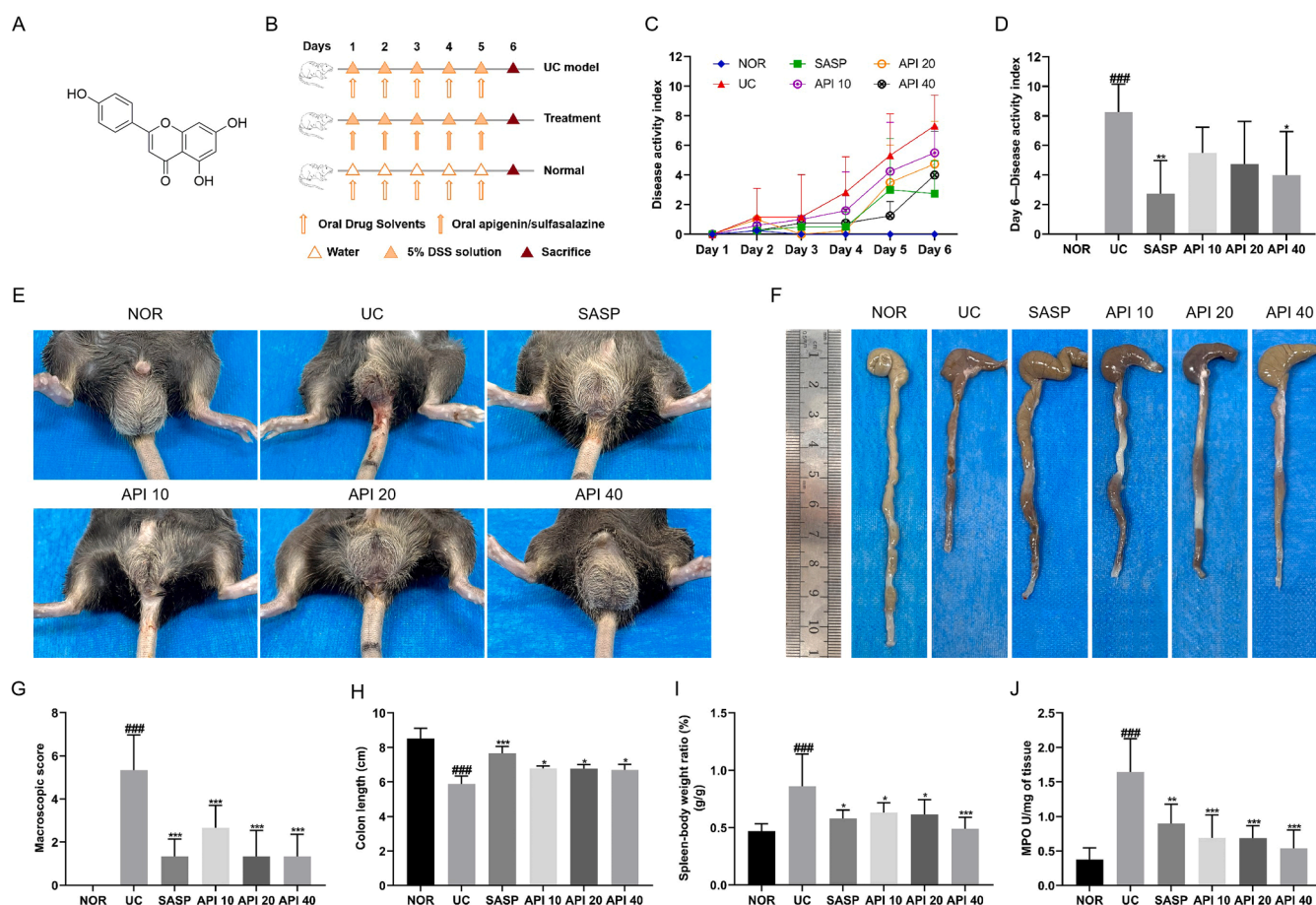


**Fig. 3.** Effect of apigenin on inflammatory symptoms in UC mice.

(A) Chemical structure of apigenin. (B) Method of establishing the mouse model of UC. (C) Disease activity index in mice. (D) Statistical analysis of the disease activity index in mice on the sixth day. (E) Representative pictures of diarrhea in each group. (F) Representative pictures of the mouse colon in each group. (G) Macroscopic scores of the mouse colon in each group. (H) The length of the mouse colon in each group. (I) The spleen-body weight ratio in each group. (J) Measurement of myeloperoxidase (MPO) activity. (vs. NOR group, ###  $p < 0.001$ ; vs. UC group, \*  $p < 0.05$ , \*\*  $p < 0.01$ , \*\*\*  $p < 0.001$ ,  $n = 6$ ).

( $5.900 \pm 0.260$  cm) was significantly shorter than that of NOR group ( $8.530 \pm 0.340$  cm). The colonic lengths of mice in both API group and SASP group were longer than those in UC group, indicating that both API and SASP can alleviate the DSS-induced colonic shortening symptoms in UC mice (Fig. 3H). By weighing the spleens and bodies of mice in each group and calculating the spleen-to-body weight ratio, it was found that this ratio in UC group was significantly higher than that in NOR group, and under the treatment of API and SASP reduced this ratio in UC mice (Fig. 3I). The results of MPO activity detection in the colonic tissues of mice in each group showed a significant increase of MPO activity in UC group. Under treatment of API and SASP, MPO activity in colonic tissues was significantly decreased, and the inhibitory effect of API on MPO activity was comparable to or superior to that of SASP (Fig. 3J). These results indicated that API had a pharmacological effect in alleviating the inflammatory symptoms of UC.

#### API inhibits UC inflammatory symptoms by suppressing the PAMP-MrgprB2-MC pro-inflammatory feedback loop

H&E staining of mouse colonic tissues showed that the colonic structure in NOR group was intact without any inflammatory pathological changes, whereas the colonic structure in UC group was severely damaged, with loss of crypt structure and multiple inflammatory cell infiltrations. Under treatment of SASP or different doses of API, the colon structure of UC mice was relatively intact, and the amount of inflammatory cell infiltration was greatly reduced (Fig. 4A). Avidin

immunofluorescence staining revealed an increase in the number of MCs in the colonic tissues of mice in UC group, accompanied by degranulation. In contrast, the infiltration and degranulation of MCs in SASP or API treated groups were reduced (Fig. 4B). Compared with the NOR group, the UC group exhibited elevated release levels of histamine and CPA3 in the colonic tissue of mice, which were markedly suppressed in response to SASP and API treatment (Figs. 4C, D). Furthermore, a notable downregulation of ADM levels was observed in the colonic tissue following API treatment (Fig. 4E). According to these results, it can be speculated that API can inhibit the infiltration and activation of MCs in the colonic tissue of UC mice, as well as the PAMP-MrgprB2-MC-regulated pro-inflammatory feedback loop.

#### API can bind to MRGPRX2 to inhibit MC activation

It was found that API can specifically bind to the active pocket of MRGPRX2, forming hydrogen bonds with amino acid residues LEU247 (2.08 Å), TRP243 (2.28 Å), and GLU246 (1.92 Å) of MRGPRX2, respectively, by the computer-simulated molecular docking technology (Fig. 5A). The Surface Plasmon Resonance (SPR) technology was employed to detect the affinity between API and MRGPRX2, and the results revealed a strong interaction between them, with a  $K_D$  value of  $67.55 \times 10^{-6}$  mol/l (Fig. 5B). In this study, calcium imaging experiments were conducted to analyze the activity of MRGPRX2 in HEK293-MRGPRX2 cells. The results of controlled experiments showed that calcium imaging buffer (CIB), PAMP-12, and 20  $\mu\text{mol/l}$  API did not

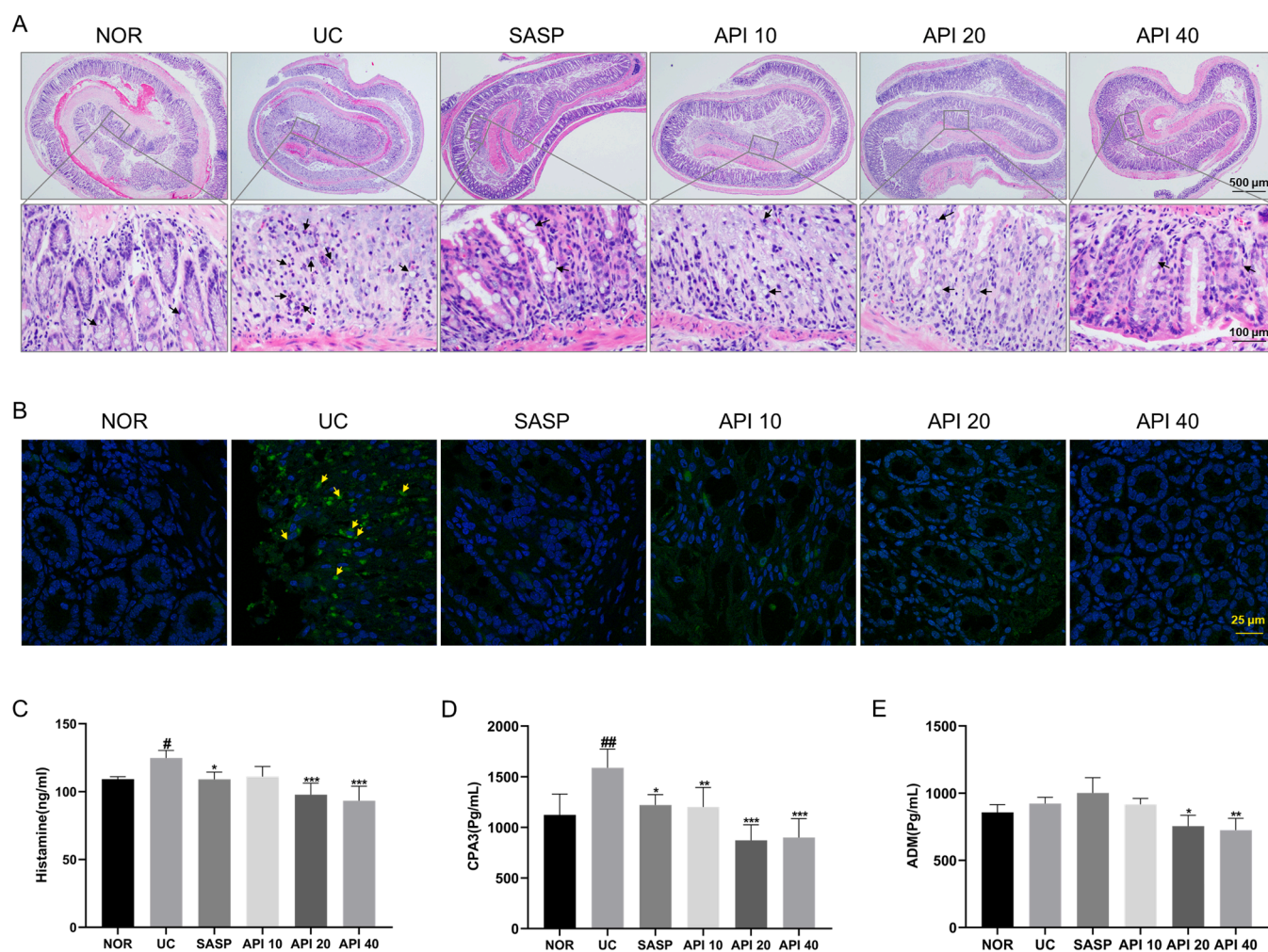


**Fig. 4.** The effect of apigenin on the damage of mouse colon tissue

(A) Structural and morphological diagrams of mouse colon tissue under the microscope, and the lower pictures were the enlarged pictures in the gray box of the upper pictures. The black arrows in the figures indicate the representative crypt structure and inflammatory cell infiltration in the colonic tissue. (B) Results of Avidin (green) and DAPI (blue) staining of mouse colon tissues. The yellow arrows marked representative avidin-stained MCs. (C) Results of histamine detection in mouse colon. (D) Detection results of CPA3 in mouse colon. (E) Detection results of ADM in mouse colon. (vs. NOR group, <sup>###</sup> $p < 0.001$ ; vs. UC group, <sup>\*</sup> $p < 0.05$ , <sup>\*\*</sup> $p < 0.01$ , <sup>\*\*\*</sup> $p < 0.001$ ,  $n = 6$ ).

trigger calcium mobilization in HEK293 cells. Furthermore, neither CIB nor 20  $\mu\text{mol/l}$  API affected calcium mobilization in HEK293-MRGPRX2 cells (Fig. 5C). API dose-dependently inhibited PAMP-12-induced  $\text{Ca}^{2+}$  influx in HEK293-MRGPRX2 cells (Fig. 5D, E). The results of calcium imaging experiments in MPMC and LAD2 cells showed that CIB had no effect on  $\text{Ca}^{2+}$  influx in either MPMC (Fig. 5F) or LAD2 (Fig. 5I) cells. API inhibited  $\text{Ca}^{2+}$  influx in PAMP-12 stimulated MPMC (Fig. 5G, H) and LAD2 (Fig. 5J, K) cells by a dose-dependent manner. Therefore, API competitively binds to MRGPRX2/B2, thereby inhibiting MC degranulation. These results indicated that API could competitively bind to MRGPRX2/B2, thereby inhibiting its activation.

Then, the levels of mediators associated with LAD2 cell activation were measured. The  $\beta$ -Hexosaminidase ( $\beta$ -Hex) release rate was  $63.12 \pm 1.41 \%$ , triggered by PAMP-12 alone, and under the treatment of 5, 10, and 20  $\mu\text{mol/l}$  of API, the  $\beta$ -Hex release rate was  $62.04 \pm 0.13 \%$ ,  $57.49 \pm 0.49 \%$ , and  $47.32 \pm 0.98 \%$ , respectively (Fig. 6A). The concentration of histamine was  $289.00 \pm 0.24 \text{ ng/ml}$  triggered by PAMP-12 alone, and under the treatment of 5, 10, and 20  $\mu\text{mol/l}$  of API, the histamine concentrations were  $265.50 \pm 1.85 \text{ ng/ml}$ ,  $256.00 \pm 0.57 \text{ ng/ml}$ , and  $238.09 \pm 2.20 \text{ ng/ml}$ , respectively (Fig. 6B). The concentration of CPA3 was  $13.26 \pm 0.74 \text{ ng/ml}$  triggered by PAMP-12 alone, and under the treatment of 5, 10, and 20  $\mu\text{mol/l}$  of API, the CPA3

concentrations were  $8.98 \pm 0.20 \text{ ng/ml}$ ,  $8.64 \pm 0.43 \text{ ng/ml}$ , and  $7.79 \pm 0.90 \text{ ng/ml}$ , respectively (Fig. 6C). The PCR experiment results demonstrated that API effectively suppressed the elevation of TNF- $\alpha$ , IL-8, and MCP-1 mRNA levels in LAD2 cells, which were induced by PAMP-12 (Fig. 6D–F). Furthermore, the ELISA results revealed that PAMP-12 can induce the release of TNF- $\alpha$ , IL-8, and MCP-1 from LAD2 cells, and notably, the release of these factors can be effectively mitigated under the treatment of API (Fig. 6G–I). These results suggested that API could inhibit PAMP-12-induced mast cell activation via MRGPRX2.

*API inhibits mast cell activation by regulating endoplasmic reticulum stress (Akt1/XBP-1S/CHOP/TXNIP) and the NF- $\kappa$ B/IL-1 $\beta$  signaling pathway*

The mRNA sequencing analysis results demonstrated that PAMP-12 triggered upregulation of 1435 genes and downregulation of 1036 genes in LAD2 cells (Fig. 7A). Concurrently, the KEGG analysis indicated that the differentially expressed genes were predominantly enriched in signaling pathways including PI3K-Akt, cytokine-cytokine receptor interaction, and cancer (Fig. 7B). Under the treatment of API, the upregulated genes in PAMP-12-activated LAD2 cells were primarily enriched in signaling pathways such as PI3K-Akt, human papillomavirus infection, and cancer (Fig. 7C, D), whereas the downregulated genes

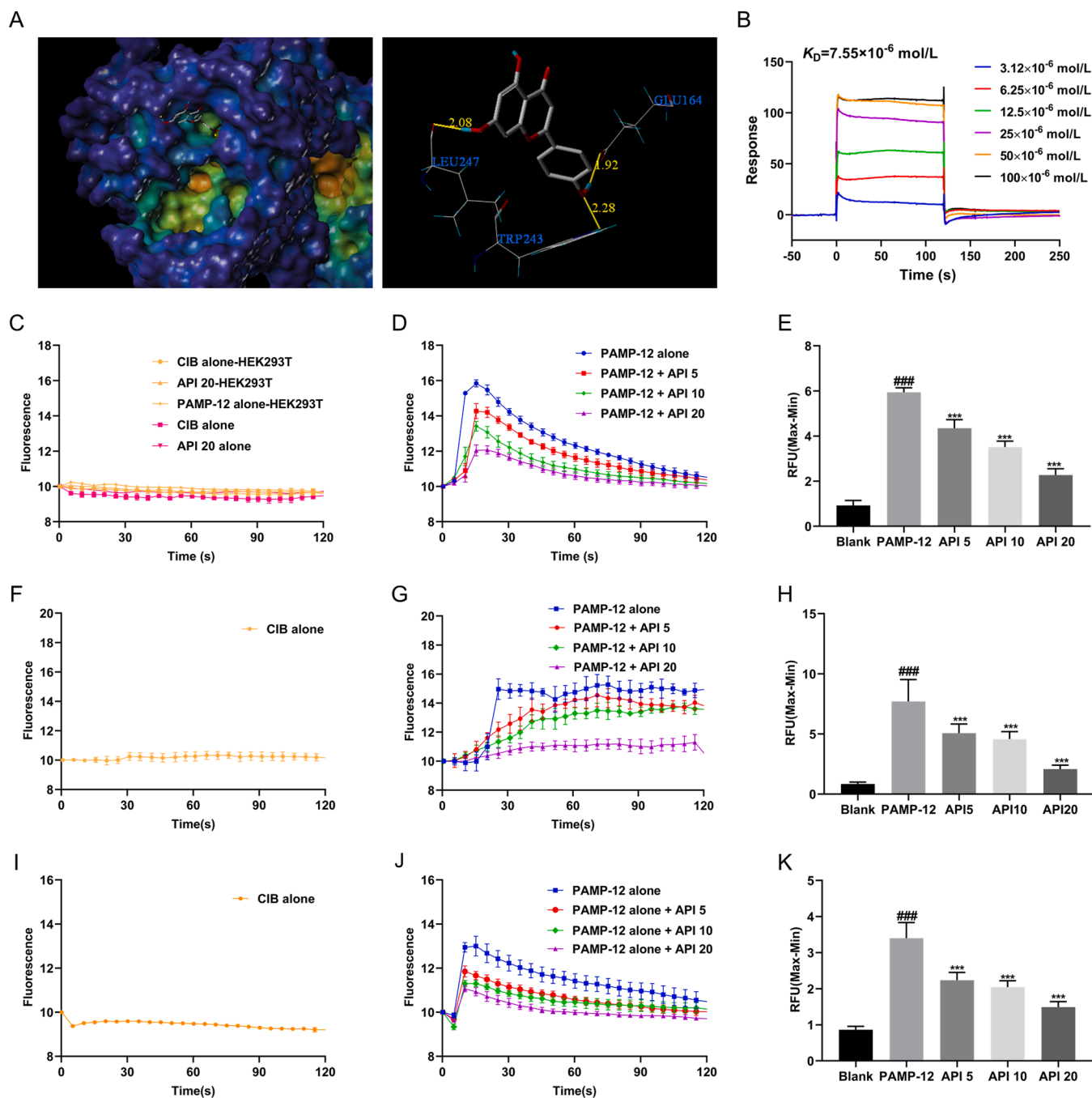


**Fig. 5.** The effect of apigenin on MRGPRX2/B2 mediated calcium inward flow in mast cells

(A) Computer simulation of apigenin and MRGPRX2 molecular docking results. The figure on the left showed the spatial binding of API with MRGPRX2 active cavities. In the right picture, API formed hydrogen bonds with MRGPRX2 amino acid residues LEU247, TRP243, and GLU164, and the bond lengths were 2.08 Å, 2.28 Å, and 1.92 Å, respectively. (B) Binding curve of apigenin and MRGPRX2 in SPR assay with a  $K_D$  of  $7.55 \times 10^{-6}$  mol/L. (C) The curves of intracellular calcium fluorescence intensity changes in HEK293 cells treated with CIB, 20  $\mu$ mol/l API, or 2  $\mu$ mol/l PAMP-12, respectively. Besides, the intracellular calcium fluorescence intensity changes in HEK293-MRGPRX2 cells were also showed, and they were treated with CIB or 20  $\mu$ mol/l API, respectively. (D) Changes in intracellular calcium fluorescence intensity of HEK293-MRGPRX2 cells pre-treated with 5  $\mu$ mol/l, 10  $\mu$ mol/l, or 20  $\mu$ mol/l API, after stimulation with PAMP-12. (E) The statistical results of the difference between the maximum and minimum values of cellular calcium fluorescence intensity in each cell of (D). (F) Curve of intracellular calcium fluorescence intensity in MPMC treated with CIB. (G) Changes in intracellular calcium fluorescence intensity of MPMC pre-treated with 5  $\mu$ mol/l, 10  $\mu$ mol/l, or 20  $\mu$ mol/l API, after stimulation with PAMP-12. (H) The statistical results of the difference between the maximum and minimum values of cellular calcium fluorescence intensity in each cell of (G). (I) Curve of intracellular calcium fluorescence intensity in LAD2 cells treated with CIB. (J) Changes in intracellular calcium fluorescence intensity of LAD2 cells pre-treated with 5  $\mu$ mol/l, 10  $\mu$ mol/l, or 20  $\mu$ mol/l API, after stimulation with PAMP-12. (K) The statistical results of the difference between the maximum and minimum values of cellular calcium fluorescence intensity in each cell of (J). (vs. Blank group (CIB alone treatment), ###  $p < 0.001$ ; vs. PAMP-12 group, \*  $p < 0.05$ , \*\*  $p < 0.01$ , \*\*\*  $p < 0.001$ ).

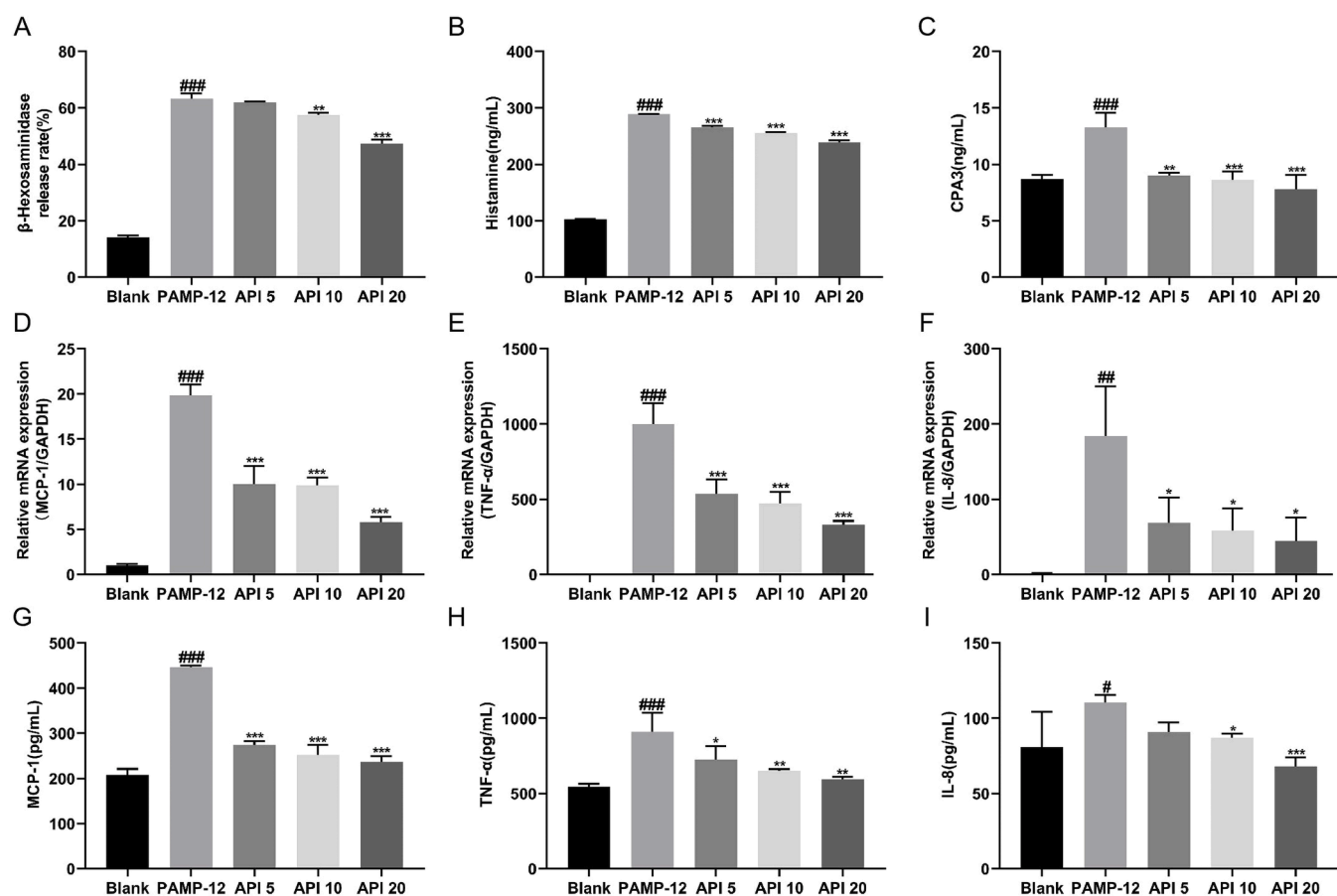


**Fig. 6.** Effect of apigenin on MRGPRX2-mediated pro-inflammatory mediator release from LAD2 cells (A)  $\beta$ -hexosaminidase release. (B) histamine release. (C) CPA3 release. (D) MCP-1 expression. (E) TNF- $\alpha$  expression. (F) IL-8 expression. (G) MCP-1 release. (H) TNF- $\alpha$  release. (I) IL-8 release. (vs. Blank group, \* $p < 0.05$ , \*\* $p < 0.01$ , \*\*\* $p < 0.001$ . vs. PAMP-12 group, \* $p < 0.05$ , \*\* $p < 0.01$ , \*\*\* $p < 0.001$ ).

were primarily enriched in molecules related to the regulation of the immune system (Fig. 7E, F). Upon conducting further screening and detailed analysis of the genes downregulated by API, it was uncovered that granzyme B (GZMB) and interleukin-17 receptor E (IL-17RE) could potentially play important roles in modulating MC activation. And, endoplasmic reticulum stress related signals may also play a vital regulatory role. Additionally, previous studies have mentioned that activated MCs could participate in tissue inflammation by secreting GZMB (Pardo et al., 2007), while IL-25, the ligand of IL-17RE, could exacerbate the severity of DSS-induced colitis (Yuan et al., 2023). The expression of each gene was verified by RT-PCR. The results showed that the mRNA expressions of ER stress related indexes CHOP, XBP-1 and TXNIP were significantly increased in PAMP-12 group compared with the blank control group, whereas it was inhibited by a dose-dependent manner under the treatment of API (Fig. 8A–C). TXNIP can regulate inflammatory responses by affecting the binding activity or transcriptional activity of NF- $\kappa$ B (P65). In the present study, API inhibited the increase in mRNA levels of IL-1 $\beta$  and NF- $\kappa$ B (P65) in LAD2 cells induced by PAMP-12 (Figure D, E), and the increase release level of GZMB triggered by PAMP-12 in LAD2 cells (Fig. 8F). Furthermore, the mRNA levels of GZMB and IL-17RE were also downregulated under the treatment of API (Fig. 8G, H).

The results of western blotting demonstrated that, under the treatment of API, the protein expression level of phosphorylated-Akt1 (p-Akt1) was upregulated in PAMP-12 triggered LAD2 cells (Fig. 9A, B). The expression levels of endoplasmic reticulum stress-related proteins CHOP, XBP-1S, and TXNIP were downregulated as the concentrations of API increased (Fig. 9A, C–E). These results suggested that API could inhibit the downstream endoplasmic reticulum stress-related CHOP/

XBP-1S/TXNIP signaling pathway by upregulating the phosphorylation level of Akt1 in PAMP-12-stimulated LAD2 cells. The NF- $\kappa$ B (P65) signaling pathway is involved in regulating the transcription and release of pro-inflammatory factors in MCs (Lei et al., 2023; Zhou et al., 2016). The phosphorylation level of NF- $\kappa$ B and the protein expression level of IL-1 $\beta$  were downregulated under the treatment of API by a dose-dependent manner (Fig. 9A, F, G), suggesting that API could downregulate NF- $\kappa$ B/IL-1 $\beta$  signaling pathway in PAMP-12-triggered MCs.

## Discussions

An investigative study revealed the existence of a pro-inflammatory positive feedback loop resulting from continuous mast cell degranulation at the inflammation site in patients with UC, thereby identifying a novel therapeutic target for UC treatment focusing on MCs and MRGPRX2 (Chen et al., 2021). However, the feasibility of this treatment strategy has not been experimentally validated. In animal models, MrgprB2 has been reported to be involved in regulating the gut microbiota composition, maintaining the gut barrier, and managing oxidative stress levels, which are associated with the pathogenesis of UC (Shao et al., 2022). In the present study, we analyzed the role of MrgprB2-mediated sustained MC degranulation in pro-inflammatory positive feedback loops in UC mice. The results indicated that both Kit<sup>W-sh/W-sh</sup> mice and MrgprB2-CKO mice exhibited notable reductions in disease progression and symptoms. This suggested that MrgprB2-mediated MC degranulation plays a crucial role in UC progression. Interestingly, a functional SP-MrgprB2 signaling axis has been found to be present in the mouse colon, and this SP-MrgprB2 signaling

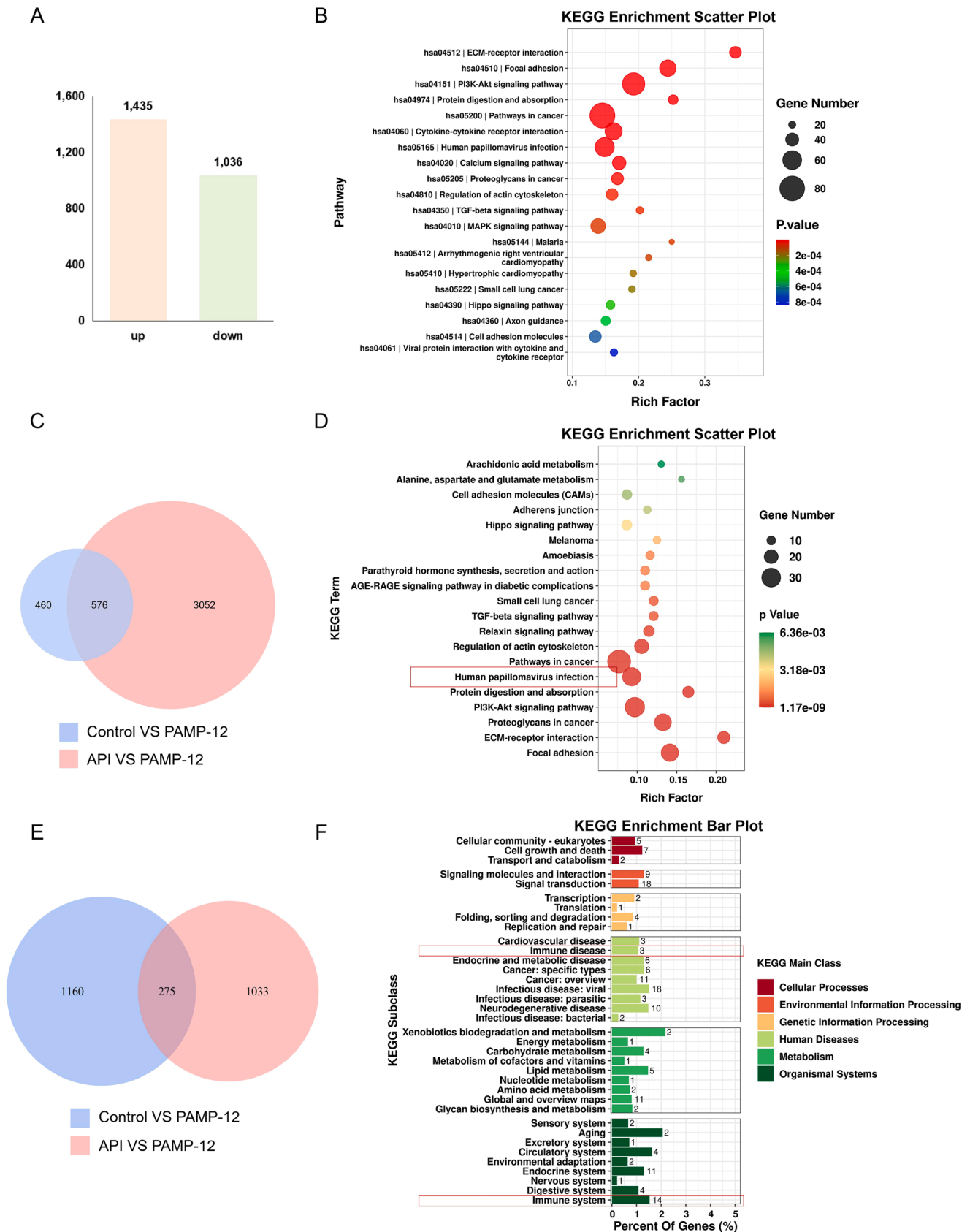


**Fig. 7.** Results of mRNA sequencing analysis of apigenin-treated LAD2 cells (A) Histogram of the number of differentially expressed up-regulated and down-regulated genes. (B) Analysis of the number of differentially expressed genes in the first 20 pathways by KEGG enrichment analysis. (C) The intersection part is the genes up-regulated by API among the genes down-regulated by PAMP-12-treated LAD2 cells. (D) KEGG pathway enrichment analysis. (E) The intersection part for genes up-regulated by API down-regulation among genes up-regulated by PAMP-12-treated LAD2 cells. (F) KEGG pathway enrichment analysis.

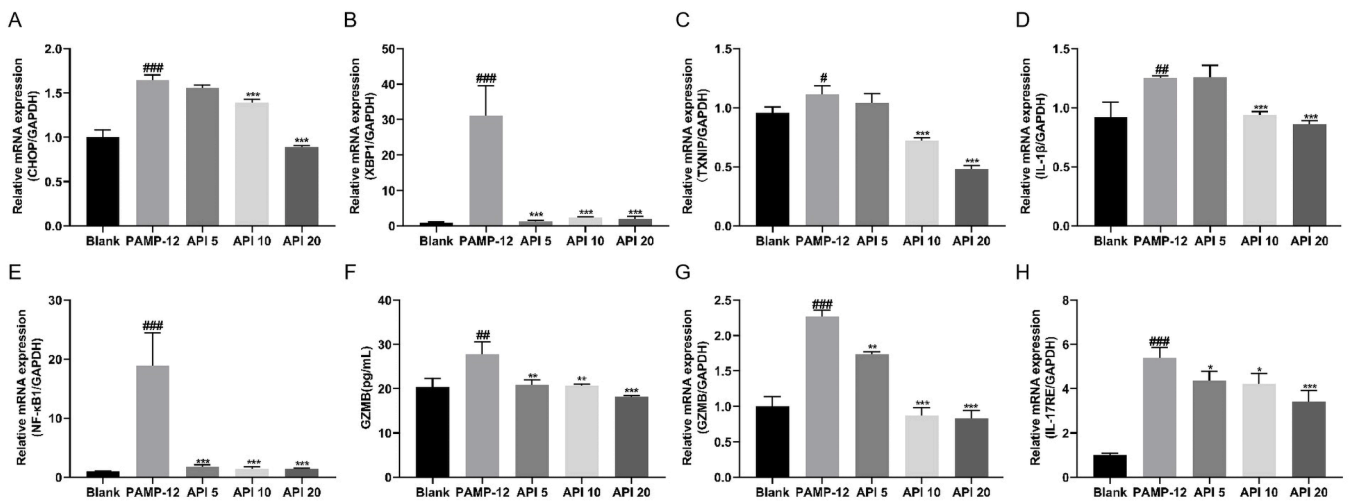


**Fig. 8.** Validation of mRNA sequencing analysis results (A) CHOP mRNA expression. (B) XBP-1 mRNA expression. (C) TXNIP mRNA expression. (D) IL-1β mRNA expression. (E) NF-κB mRNA expression. (F) GZMB release. (G) GZMB mRNA expression. and (H) IL-17RE mRNA expression. (vs. Blank group, ###*p* < 0.001; vs. PAMP-12 group, \**p* < 0.05, \*\**p* < 0.01, \*\*\**p* < 0.001).

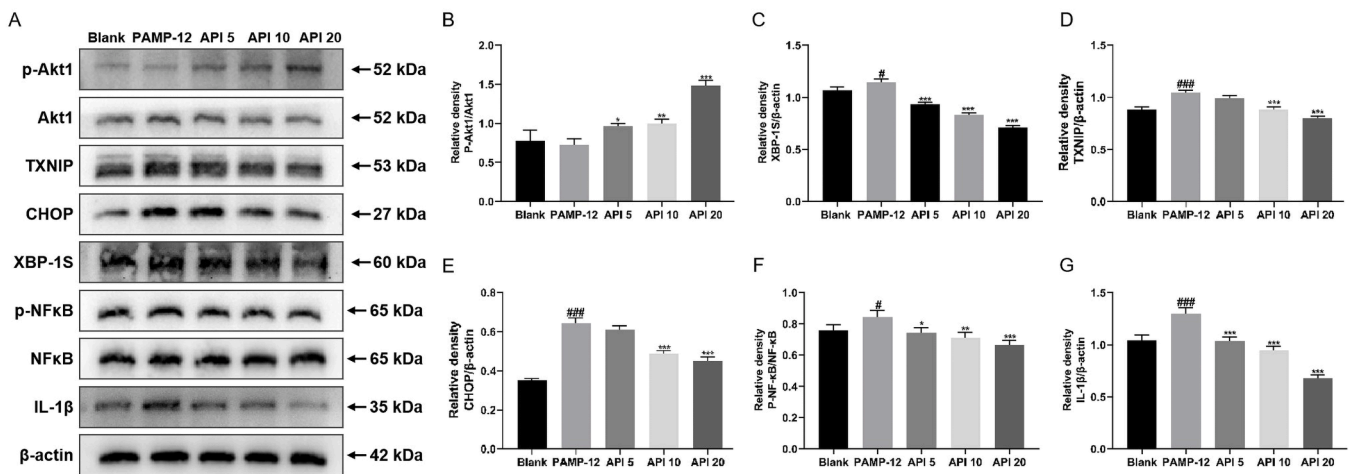


**Fig. 9.** Effect of API on the expression levels of phosphorylated Akt1, TXNIP, CHOP, XBP-1S, phosphorylated NF-κB and IL-1β proteins (A) Bar graphs of p-Akt1, Akt1, TXNIP, CHOP, XBP-1S, p-NF-κB, NF-κB, IL-1β, and β-actin proteins. The yellow arrows marked representative avidin-stained mast cells. (B) p-Akt1/Akt1 quantification results. (C) TXNIP/β-actin quantification results. (D) CHOP/β-actin quantification results. (E) XBP-1S/β-actin quantitative results. (F) p-NF-κB/NF-κB quantitative results. (G) IL-1β/β-actin quantitative results. (vs. Blank group, #*p* < 0.05, ##*p* < 0.01, ###*p* < 0.001; vs. PAMP-12 group, \**p* < 0.05, \*\**p* < 0.01, \*\*\**p* < 0.001).

contributes to degranulation of colonic MCs, affects DSS-induced neutrophil influx, and plays a defensive role in the colonic neuro-immune environment (Van Remoortel et al., 2024).

This seems to provide additional evidence for elucidating the role of MrgprB2 in colitis. The present research has showed that, in the early stages of acute UC mouse model, sustained activation of mast cells (MCs) mediated by MrgprB2 promoted inflammation progression. In addition, activating the inhibitory receptor LIMR3 or using protease inhibitors to hinder MC degranulation could potentially serve as a novel therapeutic target for inflammatory bowel disease (IBD) (Boeckstaens, 2015). This approach is consistent with our proposed method of treating UC through inhibiting MC activation via MRGPRX2/B2.

Colonic tissue MCs are primarily located within the lamina propria of the mucous membrane (Bischoff, 2009). When activated by external stimuli, MCs can exert their effects by releasing preformed mediators, such as proteases, histamine, and heparin. Alternatively, they can release de novo-synthesized mediators, including lipid mediators and cytokines, upon activation (Bischoff, 2009). These mediators engage diverse immune cells in the gut, thereby modulating the progression of

intestinal diseases (Dvornikova et al., 2023). β-Hex and CPA3 are MC-specific enzymes, and histamine is one of the important mediators pre-synthesized by MCs (Rivera and Gilfillan, 2006). In the present study, the release of inflammatory mediators in the colonic tissues of Kit<sup>W-sh/W-sh</sup> mice and MrgprB2-CKO mice decreased in the DSS-induced UC model. Specifically, we observed a reduction in the release of both CPA3, indicating a decrease in the production of the endogenous ligand PAMP-12. This suggests that the PAMP-MRGPR2/B2-mediated positive feedback loop of sustained degranulation of pro-inflammatory mediators was either blocked or attenuated. Therefore, we believe that targeting MRGPRX2 to inhibit mast cell degranulation is a novel strategy for the treatment of UC.

Currently, there are five main categories of drugs for the treatment of UC (Rogler et al., 2021). SASP is a first-line drug clinically used to treat UC and is often prescribed for widespread mild to moderately active UC, but is not effective in patients with moderate to severe UC (Rogler et al., 2021). The medicines used clinically to treat UC have limitations, such as a high incidence of adverse reactions, high usage costs, and limited treatment scope (Park and Bass, 2011; Rogler et al., 2021). It is necessary

to explore new and effective therapeutic strategies, and targeting MCs may be a promising direction in the treatment of UC.

Flavonoids exhibit a range of potential pharmacological activities, including anti-inflammatory and antioxidant effects. Certain flavonoids can counteract mast cell degranulation, thereby playing a therapeutic role in inflammatory diseases. Neohesperidin inhibits the release of mast cell-sensitizing mediators and suppresses drug allergic reactions, both *in vivo* and *in vitro* (Zhao et al., 2019). Furthermore, myricetin alleviated the symptoms of immune contact urticaria and hindered mast cell degranulation by impeding degranulation and chemokines (Hu et al., 2023). Several studies have explored the correlation between API and inflammatory symptoms in UC. For example, in acetic acid-induced UC, API facilitates the healing of ulcerative lesions and decreases the infiltration of neutrophils and other inflammatory cells (Ganjare et al., 2011). Additionally, various forms of apigenin, such as apigenin-Mn (II)-loaded sodium hyaluronate nanoparticles, API combined with glucose, and apigenin-sugar conjugates, have demonstrated promising therapeutic effects against DSS-induced UC. These treatments significantly improved colonic tissue damage, colon shortening, and myeloperoxidase levels in the colon of mice (Lv et al., 2022). However, the precise mechanisms and targets of API and its glycosides in alleviating UC remain elusive.

The present study showed that API inhibited PAMP-12-stimulated mast cell (MCs) degranulation by binding to MRGPRX2/B2, thereby preventing the release of pre-synthesized and *de novo* synthesized inflammatory mediators. MrgprB2-mediated MC degranulation contributes to the progression of UC. API blocks the PAMP-MRGPRX2-MC pro-inflammatory positive feedback loop in UC by specifically targeting MrgprB2 in MCs, thus alleviating colitis symptoms in mice. Previous studies have shown that API modulates MCs via various signaling pathways. For instance, API reduces inflammatory responses in allergic rhinitis by inhibiting the activity of the TLR4/MyD88/NF- $\kappa$ B signaling pathway in mast cells (Li et al., 2023) and inhibits the release of inflammatory mediators by blocking the NF- $\kappa$ B activation pathway in HMC-1 cells (Kang et al., 2011). Although API can regulate multiple signaling pathways, it remains unclear whether these pathways are cross-regulated by MRGPRX2. In this study, we analyzed the molecular mechanism by which API targets MRGPRX2 to inhibit mast cell degranulation. Unlike previous studies, we found that API upregulated the phosphorylation of Akt1 in LAD2 cells. Akt has a negative regulatory relationship with endoplasmic reticulum (ER) stress (Chen et al., 2023). XBP1 s is a key transcription factor and marker of ER stress, and excessive production of XBP1 s can significantly increase the release of mediators from mast cells, suggesting that XBP1 s are a target for regulating mast cell activity, such as by modulating mediator release (Fan et al., 2024). API dose-dependently inhibited the expression of ER stress markers (XBP-1S, CHOP, and TXNIP) Simultaneously, we discovered that API suppresses the activation of nuclear factor kappa B (NF- $\kappa$ B), ultimately inhibiting the maturation and release of interleukin-1 beta (IL-1 $\beta$ ) (Choi and Park, 2023). During the process of ER stress, the NLRP3 inflammasome is assembled, and activated caspase 1 is released. The activated caspase 1 promotes the maturation of IL-1 $\beta$ /IL-18 through cleavage, ultimately resulting in the development of inflammation (Choi and Park, 2023). Additionally, activated mast cells participate in tissue inflammation by secreting granzyme B (GZMB), and the interleukin-17 receptor E (IL-17RE) ligand IL-25 exacerbates the severity of dextran sulfate sodium (DSS)-induced colitis (Pardo et al., 2007; Yuan et al., 2023). We found that the API inhibited the expression of IL-17RE mRNA, as well as the expression and release of GZMB. These findings further elucidate the mechanism by which API antagonizes MCs.

Although this study has made some valuable findings in exploring treatment strategies for UC, there are still several limitations. The DSS induced mouse model of UC established in this study is an acute UC model, which is commonly used in UC research, but there are still certain differences from the pathogenesis of chronic UC in clinical

practice. Furthermore, the low homology between mouse MrgprB2 and human MRGPRX2 is often criticized. Additionally, the levels of endogenous ligands for MRGPRX2/B2 in colonic tissues, such as PAMP-12 and substance P, have not been directly detected here. In the subsequent research, the analysis of the regulatory role of MCs in chronic UC models, along with the development and application of detection methods for endogenous ligands, can provide more experimental evidence for UC treatment strategies targeting mast cell MRGPRX2/B2.

## Conclusions

In conclusion, a PAMP-MrgprB2-MC pro-inflammatory positive feedback loop was found to aggravate the inflammation progression of UC in the present research. API inhibits MC degranulation by targeting MRGPRX2/B2, thereby blocking this pro-inflammatory positive feedback loop and antagonizing UC. Additionally, API regulates the expression levels of p-Akt1, XBP-1S, CHOP, TXNIP, and the NF- $\kappa$ B/IL-1 $\beta$  signaling pathway, thus inhibiting MC degranulation. This project not only provides an experimental basis for exploring UC treatment strategies targeting MRGPRX2/B2 but also offers a promising new candidate compound for UC therapy.

## CRedit authorship contribution statement

**Yihan Huang:** Writing – original draft, Software, Project administration, Methodology, Formal analysis, Data curation. **Na Wang:** Visualization, Validation, Project administration, Data curation. **Xiaolan Ji:** Writing – original draft, Software, Project administration, Data curation. **Shiqiong Luo:** Software, Project administration, Formal analysis, Data curation. **Ling Gong:** Validation, Project administration, Data curation. **Chenrui Zhao:** Supervision, Software, Project administration, Formal analysis. **Guodong Zheng:** Project administration, Methodology, Formal analysis. **Rui Liu:** Writing – review & editing, Writing – original draft, Supervision, Project administration, Funding acquisition, Formal analysis. **Tao Zhang:** Writing – review & editing, Supervision, Conceptualization.

## Declaration of competing interest

The authors declare no competing financial interests.

## Acknowledgements

We would like to thank A. Kirshenbaum and D. Metcalfe from the National Institutes of Health (NIH, USA) for kindly providing LAD2 cells, and thank Editage ([www.editage.cn](http://www.editage.cn)) for English language editing.

## Formatting of funding sources

This work was supported by grants from the National Natural Science Foundation of China (81872837, 81903572), the Basic Research Funds for Central Universities (Grant Number: xzy012024150), and the Yulin City Science and Technology Major Special Project (YF-ZDZX-01).

## Supplementary materials

Supplementary material associated with this article can be found, in the online version, at [doi:10.1016/j.phymed.2025.156564](https://doi.org/10.1016/j.phymed.2025.156564).

## Data availability

The data that support the findings of this study are available on request from the corresponding author, [TZ or RL], upon reasonable request.

## References

- Albert-Bayo, M., Paracuellos, I., Gonzalez-Castro, A.M., Rodriguez-Urrutia, A., Rodriguez-Lagunas, M.J., Alonso-Cotoner, C., Santos, J., Vicario, M., 2019. Intestinal mucosal mast cells: key modulators of barrier function and homeostasis. *Cells* 8.
- Bawazir, M., Amponnawarat, A., Hui, Y., Oskeritziyan, C.A., Ali, H., 2022. Inhibition of MRGPRX2 but not FcεpsilonRI or MrgprB2-mediated mast cell degranulation by a small molecule inverse receptor agonist. *Front. Immunol.* 13, 1033794.
- Bischoff, S.C., 2009. Physiological and pathophysiological functions of intestinal mast cells. *Semin. Immunopathol.* 31, 185–205.
- Boeckxstaens, G., 2015. Mast cells and inflammatory bowel disease. *Curr. Opin. Pharmacol.* 25, 45–49.
- Chen, E., Chuang, L.S., Giri, M., Villaverde, N., Hsu, N.Y., Sabic, K., Joshowitz, S., Gettler, K., Nayar, S., Chai, Z., Alter, I.L., Chasteau, C.C., Korie, U.M., Dzedzik, S., Thin, T.H., Jain, A., Moscati, A., Bongers, G., Duerr, R.H., Silverberg, M.S., Brant, S. R., Rioux, J.D., Peter, I., Schumm, L.P., Haritunians, T., McGovern, D.P., Itan, Y., Cho, J.H., 2021. Inflamed ulcerative colitis regions associated with MRGPRX2-mediated mast cell degranulation and cell activation modules, defining a new therapeutic target. *Gastroenterology* 160, 1709–1724.
- Chen, J., Zheng, Z., Li, M., Cao, C., Zhou, X., Wang, B., Gan, X., Huang, Z., Liu, Y., Huang, W., Liang, F., Chen, K., Zhao, Y., Wang, X., Wu, J., Lin, L., 2023. Design, synthesis and evaluation of monoketene compounds as novel potential Parkinson's disease agents by suppressing ER stress via AKT. *Bioorg. Chem.* 136, 106543.
- Choi, E.H., Park, S.J., 2023. TXNIP: a key protein in the cellular stress response pathway and a potential therapeutic target. *Exp. Mol. Med.* 55, 1348–1356.
- de Lange, K.M., Barrett, J.C., 2015. Understanding inflammatory bowel disease via immunogenetics. *J. Autoimmun.* 64, 91–100.
- Ding, Y., Che, D., Li, C., Cao, J., Wang, J., Ma, P., Zhao, T., An, H., Zhang, T., 2019. Quercetin inhibits Mrgprx2-induced pseudo-allergic reaction via PLCγ-IP3R related Ca<sup>2+</sup> fluctuations. *Int. Immunopharmacol.* 66, 185–197.
- Dvornikova, K.A., Platonova, O.N., Bystrova, E.Y., 2023. Inflammatory bowel disease: crosstalk between histamine, immunity, and disease. *Int. J. Mol. Sci.* 24.
- Fan, J., Ma, L., Xie, B., Qiu, S., Song, S., Tang, Z., Wu, Y., Huangfu, H., Feng, Y., Luo, X., Yang, P., 2024. Modulating endoplasmic reticulum stress attenuates mast cell degranulation. *Int. Immunopharmacol.* 126, 111336.
- Feuerstein, J.D., Cheifetz, A.S., 2014. Ulcerative colitis: epidemiology, diagnosis, and management. *Mayo Clin. Proc.* 89, 1553–1563.
- Ganjare, A.B., Nirmal, S.A., Patil, A.N., 2011. Use of apigenin from *Cordia dichotoma* in the treatment of colitis. *Fitoterapia* 82, 1052–1056.
- Ginwala, R., Bhavsar, R., Chigbu, D.I., Jain, P., Khan, Z.K., 2019. Potential role of flavonoids in treating chronic inflammatory diseases with a special focus on the anti-inflammatory activity of apigenin. *Antioxidants (Basel)* 8.
- Han, S., Lv, Y., Kong, L., Che, D., Liu, R., Fu, J., Cao, J., Wang, J., Wang, C., He, H., Zhang, T., Dong, X., He, L., 2017. Use of the relative release index for histamine in LAD2 cells to evaluate the potential anaphylactoid effects of drugs. *Sci. Rep.* 7, 13714.
- Hao, Y., Che, D., Yu, Y., Liu, L., Mi, S., Zhang, Y., Hao, J., Li, W., Ji, M., Geng, S., Shi, J., 2022. Luteolin inhibits FcεpsilonRIα and MRGPRX2-mediated mast cell activation by regulating calcium signaling pathways. *Phytother. Res.* 36, 2197–2206.
- Hu, S., Zhang, Y., Dang, B., Wang, Y., Zheng, G., Zhang, T., An, H., 2023. Myricetin alleviated immunologic contact urticaria and mast cell degranulation via the PI3K/Akt/NF-κappaB pathway. *Phytother. Res.* 37, 2024–2035.
- Jeong, D.Y., Kim, S., Son, M.J., Son, C.Y., Kim, J.Y., Kronbichler, A., Lee, K.H., Shin, J.I., 2019. Induction and maintenance treatment of inflammatory bowel disease: a comprehensive review. *Autoimmun. Rev.* 18, 439–454.
- Kang, O.H., Lee, J.H., Kwon, D.Y., 2011. Apigenin inhibits release of inflammatory mediators by blocking the NF-κappaB activation pathways in the HMC-1 cells. *Immunopharmacol. Immunotoxicol.* 33, 473–479.
- Kim, J.J., Shajib, M.S., Manocha, M.M., Khan, W.I., 2012. Investigating intestinal inflammation in DSS-induced model of IBD. *J. Vis. Exp.*
- Lei, F., Wu, Y., Li, C., Yan, B., Chen, S., Peng, Q., Yang, X., Ma, P., 2023. Mediation of endoplasmic reticulum stress and NF-κappaB signaling pathway in DNP-exacerbated allergic asthma: a toxicological study with Balb/c mice. *J. Hazard. Mater.* 460, 132392.
- Li, H., Zhang, H., Zhao, H., 2023. Apigenin attenuates inflammatory response in allergic rhinitis mice by inhibiting the TLR4/MyD88/NF-κappaB signaling pathway. *Environ. Toxicol.* 38, 253–265.
- Li, M., Weigmann, B., 2023. Effect of a flavonoid combination of apigenin and epigallocatechin-3-gallate on alleviating intestinal inflammation in experimental colitis models. *Int. J. Mol. Sci.* 24.
- Lilla, J.N., Chen, C.C., Mukai, K., BenBarak, M.J., Franco, C.B., Kalesnikoff, J., Yu, M., Tsai, M., Piliponsky, A.M., Galli, S.J., 2011. Reduced mast cell and basophil numbers and function in Cpa3-cre; Mcl-1fl/fl mice. *Blood* 118, 6930–6938.
- Liu, R., Che, D.L., Zhao, T.T., Pundir, P., Cao, J., Lv, Y.N., Wang, J., Ma, P.Y., Fu, J., Wang, N.N., Wang, X.Y., Zhang, T., Dong, X.Z., He, L.C., 2017. MRGPRX2 is essential for sinomenine hydrochloride induced anaphylactoid reactions. *Biochem. Pharmacol.* 146, 214–223.
- Lv, F., Zhang, Y., Peng, Q., Zhao, X., Hu, D., Wen, J., Liu, K., Li, R., Wang, K., Sun, J., 2022. Apigenin-Mn(II) loaded hyaluronic acid nanoparticles for ulcerative colitis therapy in mice. *Front. Chem.* 10, 969962.
- Madunic, J., Madunic, I.V., Gajski, G., Popic, J., Garaj-Vrhovac, V., 2018. Apigenin: a dietary flavonoid with diverse anticancer properties. *Cancer Lett.* 413, 11–22.
- McNeil, B.D., Pundir, P., Meeker, S., Han, L., Udem, B.J., Kulka, M., Dong, X., 2015. Identification of a mast-cell-specific receptor crucial for pseudo-allergic drug reactions. *Nature* 519, 237–241.
- Mowat, C., Cole, A., Windsor, A., Ahmad, T., Arnott, I., Driscoll, R., Mitton, S., Orchard, T., Rutter, M., Younge, L., Lees, C., Ho, G.T., Satsangi, J., Bloom, S., Gastroenterology, I.B.D.S.o.t.B.S.o., 2011. Guidelines for the management of inflammatory bowel disease in adults. *Gut* 60, 571–607.
- Pardo, J., Wallich, R., Ebneth, K., Iden, S., Zentgraf, H., Martin, P., Ekciler, A., Prins, A., Mullbacher, A., Huber, M., Simon, M.M., 2007. Granzyme B is expressed in mouse mast cells *in vivo* and *in vitro* and causes delayed cell death independent of perforin. *Cell Death Differ.* 14, 1768–1779.
- Park, K.T., Bass, D., 2011. Inflammatory bowel disease-attributable costs and cost-effective strategies in the United States: a review. *Inflamm. Bowel Dis.* 17, 1603–1609.
- Rijnierse, A., Nijkamp, F.P., Kraneveld, A.D., 2007. Mast cells and nerves tickle in the tummy: implications for inflammatory bowel disease and irritable bowel syndrome. *Pharmacol. Ther.* 116, 207–235.
- Rivera, J., Gilfillan, A.M., 2006. Molecular regulation of mast cell activation. *J. Allergy Clin. Immunol.* 117, 1214–1225; quiz 1226.
- Rogler, G., Singh, A., Kavanaugh, A., Rubin, D.T., 2021. Extraintestinal manifestations of inflammatory bowel disease: current concepts, treatment, and implications for disease management. *Gastroenterology* 161, 1118–1132.
- Salehi, B., Venditti, A., Sharifi-Rad, M., Kregiel, D., Sharifi-Rad, J., Durazzo, A., Lucarini, M., Santini, A., Souto, E.B., Novellino, E., Antolak, H., Azzini, E., Setzer, W. N., Martins, N., 2019. The therapeutic potential of apigenin. *Int. J. Mol. Sci.* 20.
- Shao, M., Yuan, F., Liu, J., Luo, H., 2022. Mast cell specific receptor Mrgprb2 regulating experimental colitis is associated with the microbiota-gut-brain axis. *J. Inflamm. Res.* 15, 6137–6151.
- Turner, D., Ricciuto, A., Lewis, A., D'Amico, F., Dhaliwal, J., Griffiths, A.M., Bettenworth, D., Sandborn, W.J., Sands, B.E., Reinisch, W., Scholmerich, J., Bemelman, W., Danese, S., Mary, J.Y., Rubin, D., Colombel, J.F., Peyrin-Biroulet, L., Dotan, I., Abreu, M.T., Dignass, A., International Organization for the Study of I.B.D., 2021. STRIDE-II: an update on the selecting therapeutic targets in Inflammatory Bowel Disease (STRIDE) Initiative of the International Organization for the Study of IBD (IOIBD): determining therapeutic goals for treat-to-target strategies in IBD. *Gastroenterology* 160, 1570–1583.
- Van Remoortel, S., Lambrechts, L., De Winter, B., Dong, X., Rodriguez Ruiz, J.P., Kumar-Singh, S., Martinez, S.L., Timmermans, J.P., 2024. Mrgprb2-dependent mast cell activation plays a crucial role in acute colitis. *Cell Mol. Gastroenterol. Hepatol.* 101391
- Wehkamp, J., Gotz, M., Herrlinger, K., Steurer, W., Stange, E.F., 2016. Inflammatory bowel disease. *Dtsch. Arztebl. Int.* 113, 72–82.
- Wirtz, S., Neufert, C., Weigmann, B., Neurath, M.F., 2007. Chemically induced mouse models of intestinal inflammation. *Nat. Protoc.* 2, 541–546.
- Wirtz, S., Popp, V., Kindermann, M., Gerlach, K., Weigmann, B., Fichtner-Feigl, S., Neurath, M.F., 2017. Chemically induced mouse models of acute and chronic intestinal inflammation. *Nat. Protoc.* 12, 1295–1309.
- Wu, H., Zeng, M., Cho, E.Y., Jiang, W., Sha, O., 2015. The origin, expression, function and future research focus of a G protein-coupled receptor, mas-related gene X2 (MrgX2). *Prog. Histochem. Cytochem.* 50, 11–17.
- Yan, Y.X., Shao, M.J., Qi, Q., Xu, Y.S., Yang, X.Q., Zhu, F.H., He, S.J., He, P.L., Feng, C.L., Wu, Y.W., Li, H., Tang, W., Zuo, J.P., 2018. Artemisinin analogue SM934 ameliorates DSS-induced mouse ulcerative colitis via suppressing neutrophils and macrophages. *Acta Pharmacol. Sin.* 39, 1633–1644.
- Yang, F., Guo, L., Li, Y., Wang, G., Wang, J., Zhang, C., Fang, G.X., Chen, X., Liu, L., Yan, X., Liu, Q., Qu, C., Xu, Y., Xiao, P., Zhu, Z., Li, Z., Zhou, J., Yu, X., Gao, N., Sun, J.P., 2021. Structure, function and pharmacology of human itch receptor complexes. *Nature* 600, 164–169.
- Yuan, Q., Peng, N., Xiao, F., Shi, X., Zhu, B., Rui, K., Tian, J., Lu, L., 2023. New insights into the function of Interleukin-25 in disease pathogenesis. *Biomark. Res.* 11, 36.
- Zhao, T., Hu, S., Ma, P., Che, D., Liu, R., Zhang, Y., Wang, J., Li, C., Ding, Y., Fu, J., An, H., Gao, Z., Zhang, T., 2019. Neohesperidin suppresses IgE-mediated anaphylactic reactions and mast cell activation via lyn-PLC-Ca<sup>2+</sup> pathway. *Phytother. Res.* 33, 2034–2043.
- Zhou, Q., Wang, H., Schwartz, D.M., Stoffels, M., Park, Y.H., Zhang, Y., Yang, D., Demirkaya, E., Takeuchi, M., Tsai, W.L., Lyons, J.J., Yu, X., Ouyang, C., Chen, C., Chin, D.T., Zaal, K., Chandrasekharappa, S.C., Hanson, E.P., Yu, Z., Mullikin, J.C., Hasni, S.A., Wertz, I.E., Ombrello, A.K., Stone, D.L., Hoffmann, P., Jones, A., Barham, B.K., Leavis, H.L., van Royen-Kerkof, A., Sibley, C., Batu, E.D., Gul, A., Siegel, R.M., Boehm, M., Milner, J.D., Ozen, S., Gadinia, M., Chae, J., Laxer, R.M., Kastner, D.L., Aksentjevich, I., 2016. Loss-of-function mutations in TNFAIP3 leading to A20 haploinsufficiency cause an early-onset autoinflammatory disease. *Nat. Genet.* 48, 67–73.